

Beyond y and μ : the shape of the CMB spectral distortions in the intermediate epoch, $1.5 \times 10^4 \lesssim z \lesssim 2 \times 10^5$

Rishi Khatri,^a Rashid A. Sunyaev^{a,b,c}

^aMax Planck Institut für Astrophysik
, Karl-Schwarzschild-Str. 1 85741, Garching, Germany

^bSpace Research Institute, Russian Academy of Sciences, Profsoyuznaya 84/32, 117997 Moscow, Russia

^cInstitute for Advanced Study, Einstein Drive, Princeton, New Jersey 08540, USA

E-mail: khatri@mpa-garching.mpg.de

Abstract. We calculate numerical solutions and analytic approximations for the intermediate-type spectral distortions. Detection of a μ -type distortion (saturated comptonization) in the CMB will constrain the time of energy injection to be at a redshift $2 \times 10^6 \gtrsim z \gtrsim 2 \times 10^5$, while a detection of a y -type distortion (minimal comptonization) will mean that there was heating of CMB at redshift $z \lesssim 1.5 \times 10^4$. We point out that the partially comptonized spectral distortions, generated in the redshift range $1.5 \times 10^4 \lesssim z \lesssim 2 \times 10^5$, are much richer in information than the pure y and μ -type distortions. The spectrum created during this period is intermediate between y and μ -type distortions and depends sensitively on the redshift of energy injection. These intermediate-type distortions cannot be mimicked by a mixture of y and μ -type distortions at all frequencies and vice versa. The measurement of these intermediate-type CMB spectral distortions has the possibility to constrain precisely not only the amount of energy release in the early Universe but also the mechanism, for example, particle annihilation and Silk damping can be distinguished from particle decay. The intermediate-type distortion templates and software code using these templates to calculate the CMB spectral distortions for user-defined energy injection rate are made publicly available.

Keywords: cosmic background radiation — cosmology:theory — early universe —

Contents

1	Introduction	1
2	Possible non-standard sources of energy injection in the early Universe	3
3	Definition of CMB reference temperature and spectral distortion	3
4	Creation of y-type distortion, role of Compton y_γ parameter and validity of the solution	5
4.1	Compton parameter y_γ and the Compton distortion parameter y .	5
5	Evolution of y-type distortion	9
5.1	Numerical solution in the intermediate era, $1.5 \times 10^4 \lesssim z \lesssim 2 \times 10^5$	10
5.2	Analytic solution in the weak comptonization limit	11
6	Application: Amplitude, slope and shape of the primordial power spectrum on small scales	13
7	Application: annihilation and decay of particles	18
8	Non-degeneracy among Intermediate-type distortions and a mixture of y and μ-type distortions	20
9	Observational issues	22
10	Conclusions	23
A	Fitting formulae for x_0, x_{\min}, x_{\max} as a function of y_γ	28
B	Analytic approximate solutions of Kompaneets equation	29
C	Corrections to y-type distortion from weak comptonization and recursion relations for calculating the higher order terms	31

1 Introduction

Cosmic background explorer (COBE/FIRAS) [1] measurements show that cosmic microwave background (CMB) follows Planck spectrum to a high precision between $1 < x < 11$, where $x = h\nu/k_B T$ is the dimensionless frequency, h is Planck's constant, k_B is Boltzmann's constant and T is the temperature of the CMB blackbody spectrum. The precision is quantified by the 2σ limits on the chemical potential [2] $\mu \lesssim 9 \times 10^{-5}$ and y -type distortion [3] $y \lesssim 1.5 \times 10^{-5}$. Technologically an improvement of more than two orders of magnitude over COBE/FIRAS has been possible for some time [4] and proposed future experiment Primordial Inflation Explorer (PIXIE) [5] will be able to measure a y -type distortion of $y = 10^{-8}$ or $\mu = 5 \times 10^{-8}$ at 5σ , a more than three orders of magnitude improvement over COBE/FIRAS.

In case there is energy or photon production at a redshift $z \gtrsim 2 \times 10^6$, the photon production and destruction through bremsstrahlung and double Compton scattering along with the redistribution of

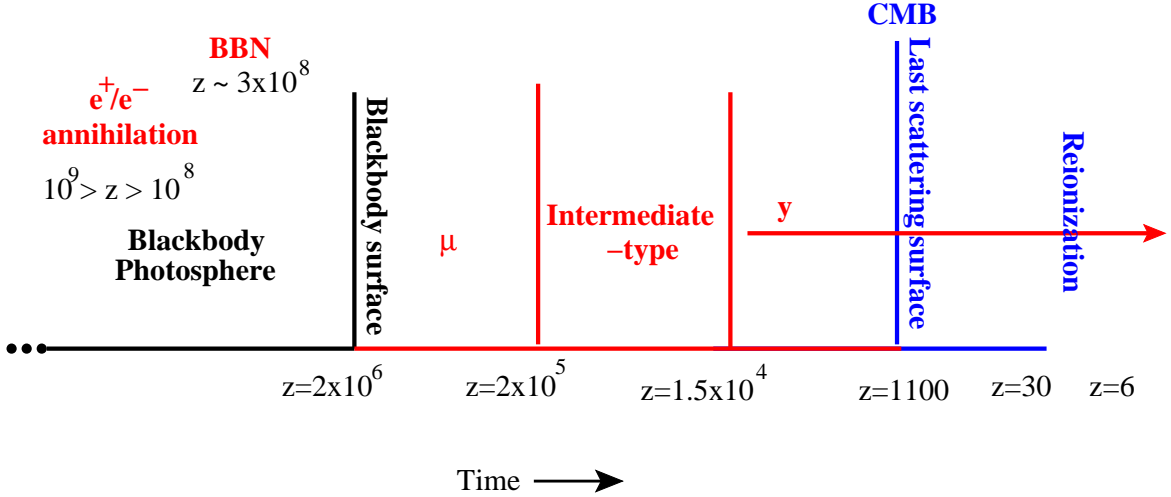


Figure 1. Important epochs related to the creation and evolution of the CMB spectrum.

photons in energy via Compton scattering on thermal electrons can establish full thermal equilibrium [2, 6, 7] and we get a blackbody spectrum with a higher temperature. The redshift $z \approx 2 \times 10^6$ therefore defines the boundary of the blackbody photosphere. This happens, for example, when electrons and positrons, having higher initial entropy and energy density than photons, annihilate at $z \sim 10^8 \sim 10^9$. Also, when there is energy release during primordial nucleosynthesis, the photon spectrum quickly thermalizes. For redshifts between $2 \times 10^5 \lesssim z \lesssim 2 \times 10^6$, any heating of CMB gives rise to a Bose-Einstein spectrum or a μ -type distortion, where μ is the chemical potential. For redshifts $z \lesssim 1.5 \times 10^4$, the Compton redistribution of photons over frequencies is too weak to establish the equilibrium Bose-Einstein spectrum and we get a y -type spectrum. For μ -type (y -type) distortions, if detected, we can only put a lower (upper) limit to the time of energy release. However, if there is heating of CMB in the redshift range $1.5 \times 10^4 \lesssim z \lesssim 2 \times 10^5$, the spectrum depends sensitively on the time of energy injection and it is thus possible to put a much more precise constraint on the time of energy release. Important epochs in the history of the early Universe, from point of view of the CMB spectrum, are depicted schematically in Fig. 1.

We first define the spectral distortion as a pure redistribution of photons of a reference blackbody, which is slightly different for μ type distortions from the conventional definition. This definition makes it possible to uniquely define the zero point/crossing frequency of the spectral distortion and use it to determine the redshift of energy injection. We review the y -type solution and also calculate the regime of validity of this solution in the Appendices. We study the comptonization of y -type distortion and calculate the evolution of zero point/crossing frequency of the distortion. As a first example, we discuss the shape of the spectral distortions arising from the dissipation of sound waves in the early Universe [8–14] and how they can be used to constrain the shape of the primordial power spectrum on small scales with wavenumbers $8 < k < 378 \text{ Mpc}^{-1}$. Additional significant sources of heating/cooling in the early Universe include dark matter (WIMP) annihilation and adiabatic cooling of baryons [12, see also 7, 15]. The y -type distortions are also created throughout the late-time history of the universe, in particular from the heating of CMB by hotter electrons in the intergalactic medium during and after reionization, and by hot intracluster electrons in the clusters of galaxies. The early Universe contributions to the y -type distortions, before recombination, are indistinguishable from the late-time contributions; y -type distortions are therefore not very useful in constraining possible new physics, which can heat the CMB before reionization. As long as the distortions are small, the y -type

distortions from different epochs and the μ and the intermediate-type distortions just add linearly to give the total distortion to the CMB. Evolution of spectral distortions in the early Universe was first considered by Zeldovich and Sunyaev [2, 3] and analytic and numerical solutions were computed by [16]. These and later calculations [6, 12, 17–19], which included double Compton scattering and considered low baryon density Universes such as ours, were focused on μ and y -type distortions, although some authors computed the full evolution of the spectrum, including intermediate-type contributions. We should clarify that in this paper we are always in the non-relativistic regime and are not concerned about the relativistic corrections to either the Kompaneets equation [20] or the y -type distortions, which have been studied in some detail by various authors [21–32] in applications to the very hot ($T_e \gtrsim 10$ KeV) gas inside clusters of galaxies.

In the following calculations we will use WMAP cosmological parameters of Λ CDM cosmology [33] with CMB temperature today $T_{\text{CMB}} = 2.725\text{K}$, number of neutrinos $N_\nu = 3.046$ [34], helium mass fraction $y_{He} = 0.24$, Hubble constant $H_0 = 70.2\text{km/s/Mpc}$, matter density $\Omega_m = 0.275$, baryon density $\Omega_b = 0.0458$ and zero curvature.

2 Possible non-standard sources of energy injection in the early Universe

Detection of energy release in the early Universe is an important source of information about new physics. There are several possible theoretical sources from high energy theories. For example, in super-symmetric theories and Kaluza-Klein theories it is possible that dark matter was initially produced as a long lived next to lightest particle in the dark sector and then decays later to the lightest particle which acts as dark matter today [35]. An example is a neutralino (\tilde{B}) decaying to gravitino (\tilde{G}) in super-symmetric theories. Neutralino in this case is a WIMP which decays into gravitino which has only gravitational interaction is thus super weakly interacting or SWIMP [36]. Sterile neutrinos can also be a significant component of dark matter and their decay can be a source of energy and photons [35]. Other sources of energy release include evaporating primordial black holes [37], decaying cosmic strings and other topological defects, cosmic string wakes [38] and oscillating super-conducting cosmic strings [39, 40], and small-scale primordial magnetic fields [41].

In most of the above examples the decay of an initial particle results in high energy electromagnetic and hadronic showers. Initial standard model particles, that are produced as a result of these showers, interact with electrons, ions and photons through a rich variety of energetic processes like Compton and inverse Compton scattering, pair production, photon-photon interaction etc. (see for example [42]) depositing most of the initial energy in the form of heat in plasma very quickly. Some of the energy is lost to neutrinos and energetic particles in the windows of low optical depth. This energy deposition in turn gives rise to a y -type distortion which then comptonizes. As a second example, we consider decay of an unstable particle as a source of energy injection and show how the intermediate-type spectral distortions can constrain the life time of the particle as well as distinguish it from energy injection due to a process for which the rate of energy injection as a function of redshift is not exponential but a power law, such as annihilation of particles or dissipation of sound waves.

3 Definition of CMB reference temperature and spectral distortion

For any given isotropic unpolarized photon spectrum, $n(\nu)$, where n is the occupation number as a function of frequency ν , we can define a unique reference temperature. At redshifts $z \lesssim 2 \times 10^6$, the energy exchange between the plasma and radiation is very fast, but the production (and absorption) of photons is extremely slow. As a result, the number density of photons does not change due to energy

release and the ratio of photon to baryon number density n_γ/n_b is constant to high precision.¹ We can calculate the total number density of photons in the spectrum

$$N = \int \frac{8\pi\nu^2}{c^3} n(\nu) d\nu, \quad (3.1)$$

where c is the speed of light. We can now define a reference temperature, T , as the temperature of the blackbody spectrum n_{pl} which has the same number density N . Thus $T = (N/b_R)^{1/3}$, where $b_R = \frac{16\pi k_B^3 \zeta(3)}{c^3 h^3}$, ζ is the Riemann zeta function with $\zeta(3) \approx 1.20206$. We can now also define dimensionless frequency, $x = h\nu/(k_B T)$ and write the total spectrum as

$$n(x) = n_{\text{pl}}(x) + \Delta n(x), \quad (3.2)$$

where Δn is the distortion from the reference blackbody with the property that it represents a redistribution of photons in the reference blackbody, $n_{\text{pl}} = 1/(e^x - 1)$. The total number of photons in the distortion vanishes, $\int dx x^2 \Delta n \equiv 0$. This formalism is especially useful for discussing the distortions created in the early Universe solely through the action of comptonization, which just redistributes the photons already existing in a previous spectrum, and thus does not change the reference temperature defined above. Of course, many other definitions of spectral distortions are possible by defining a different reference temperature [12, 13]. The above definition is just an extension of the conventional definition of a y -type distortion to distortion of any shape.

In the rest of the paper we will use the above definitions of reference temperature and spectral distortions. We note that for the case of a Bose-Einstein spectrum n_{BE} , the above definition gives a different reference temperature than the one given by the usual definition $n_{\text{BE}} = 1/(e^{\frac{h\nu}{k_B T_{\text{BE}}} + \mu} - 1)$. Let us remind that n_{BE} is the equilibrium solution of the Kompaneets equation [20] when $T_e = T_{\text{BE}}$, where T_e is the electron temperature. Our definition corresponds to taking an initial blackbody spectrum with temperature equal to the reference temperature T and add to it small amount of energy (keeping the photon number constant), which then fully comptonizes creating a Bose-Einstein spectrum with a chemical potential μ fully defined by the amount of energy release. It is easy to calculate the final temperature of the resulting spectrum using relations for number density and energy density of a Bose-Einstein spectrum in the limit of small chemical potential [44] and it is given by $t \equiv (T_{\text{BE}} - T)/T = 0.456\mu$. Thus the spectrum written in terms of dimensionless frequency $x = h\nu/k_B T$ is given by,

$$\begin{aligned} n_{\text{BE}} &= \frac{1}{e^{\frac{h\nu}{k_B T_{\text{BE}}} + \mu} - 1} \\ &= \frac{1}{e^{x-0.456\mu x + \mu} - 1} \\ &\approx n_{\text{pl}}(x) + \frac{\mu e^x}{(e^x - 1)^2} \left(\frac{x}{2.19} - 1 \right), \end{aligned} \quad (3.3)$$

giving the zero point, where the coefficient of μ in above equation vanishes making the spectrum identical to the blackbody spectrum at temperature T , at $x_0 = 2.19, \nu = 124$ GHz, compared to $x_0 = 3.83, \nu = 217$ GHz for a y -type distortion [3],

$$n_y(x) = \frac{x e^x}{(e^x - 1)^2} \left[x \left(\frac{e^x + 1}{e^x - 1} \right) - 4 \right]. \quad (3.4)$$

¹There is an exception, of course, when the energy release mechanism also adds photons, for example Silk damping [13, 43].

Finally we note that part of the energy release from sound wave dissipation in the early Universe goes into blackbody part of the spectrum [13]. The blackbody part of the energy release is easily absorbed in the reference temperature T and can be ignored completely in our method, where we define the spectral distortions as pure redistribution of photons of a reference blackbody.² We have plotted in Fig2. y -type and μ -type (Bose-Einstein) distortions having same number and energy density. The fractional difference in the effective temperature is plotted, which is defined by the following equations.

$$\begin{aligned} n(x) &\equiv \frac{1}{e^{h\nu/k_B T_{\text{eff}}(x)} - 1} \\ &= \frac{1}{e^{xT/T_{\text{eff}}(x)} - 1} \\ \Rightarrow \frac{\Delta T}{T} &\equiv \frac{T_{\text{eff}} - T}{T} \approx \frac{1 - e^{-x}}{x} \frac{\Delta n}{n_{\text{pl}}}. \end{aligned} \quad (3.5)$$

Fig. 3 shows the difference in intensity from blackbody, $\Delta I_\nu \equiv I_\nu^{\mu,y} - I_\nu^{\text{pl}} \propto x^3 \Delta n$, where $I_\nu^{\mu,y}$ is the intensity of μ or y distorted spectrum, and I_ν^{pl} is the intensity of Planck spectrum at reference temperature T defined above. The two type of distortions shown (μ and y) have the same energy density.

4 Creation of y -type distortion, role of Compton y_γ parameter and validity of the solution

A source of energy injection, for example dark matter decay, will in general lead to a shower of particles which will quickly deposit most of their energy in the plasma, and result in an increase in the electron temperature as long as the source is on. We will first review the y -type distortions created as a result of a source of energy that turns on for a very short time and also discussed the regime of validity of this solution.

4.1 Compton parameter y_γ and the Compton distortion parameter y .

The equation describing the evolution of photon spectrum through Compton scattering is the Kompaneets equation [20]. We will work with the dimensionless frequency x and the photon occupation number $n(x)$ which is given in the case of blackbody spectrum at temperature $T = 2.725(1+z)$ K by $n_{\text{pl}}(x) = 1/(e^x - 1)$. In the case of a blackbody or a Bose-Einstein spectrum at a different temperature, there will be factors associated with the rescaling of temperature. Working with $n(x)$, which is invariant with respect to the adiabatic expansion of photon gas, allows us to avoid the extra terms in the equations associated with the expansion of the Universe. To simplify equations further, we will use as our time variable the parameter y_γ (not to be confused with the y -type distortion parameter y) defined as follows:

$$y_\gamma(z, z_{\text{max}}) = - \int_{z_{\text{max}}}^z dz \frac{k_B \sigma_T}{m_e c} \frac{n_e T}{H(1+z)}, \quad (4.1)$$

²If we add of order ϵ fractional energy to a blackbody of initial temperature T with part of it going into blackbody and part into μ distortion, then for the new temperature T' we have, $(T' - T)/T \sim \mu \sim \epsilon$. Ignoring the energy addition to the blackbody part we will use the frequency variable x , while the frequency variable with respect to the new reference temperature is $x' = h\nu/(k_B T')$. The error introduced in the calculation of distortions is thus second order in ϵ , $\Delta n(x)/n(x) = \Delta n(x')/n(x') + O(\epsilon^2)$, and can be ignored for small distortions. In addition, this change in blackbody temperature takes no part in comptonization, since it also changes the electron temperature by the same amount (Eq. (5.1)).

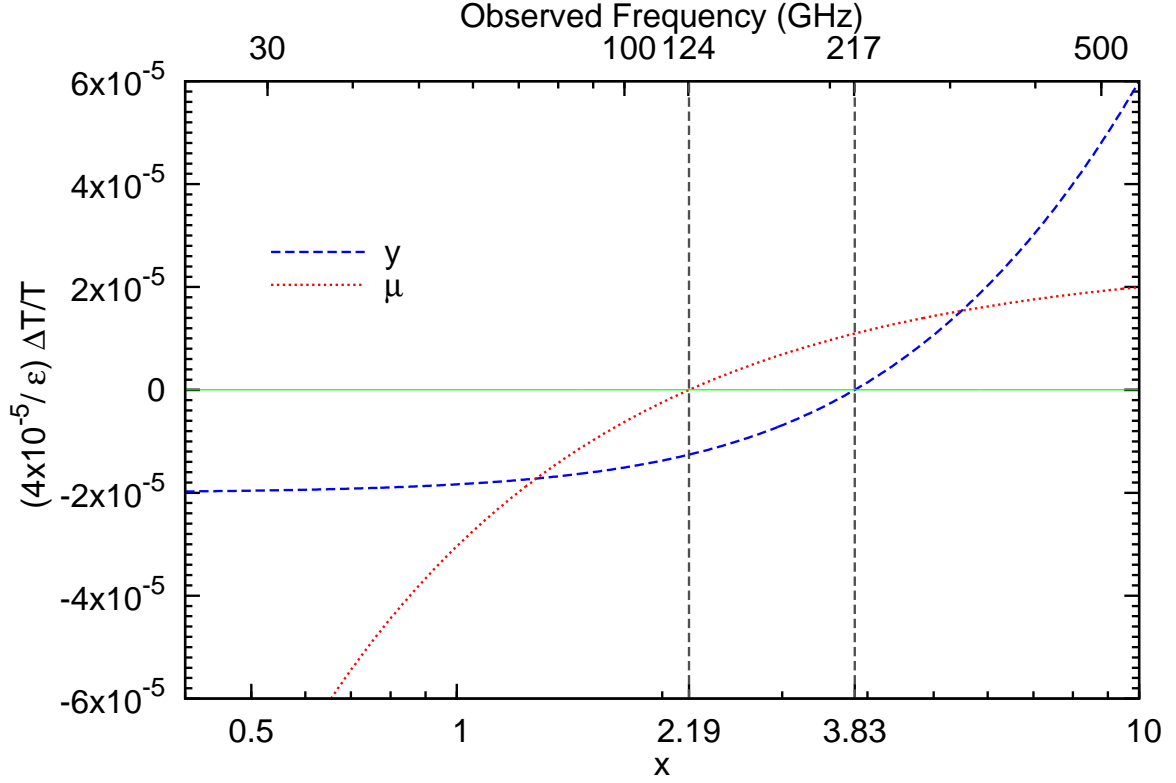


Figure 2. y -type and μ -type distortions created by addition of energy $\mathcal{E} \equiv \Delta E/E = 4 \times 10^{-5}$ to a blackbody with reference temperature T . Fractional difference in effective temperature defined in Eq. 3.5 is plotted.

where z_{\max} is the redshift where we start the evolution of the spectrum or the energy injection redshift. It is convenient to use radiation temperature T and not electron temperature T_e in the definition of x and y_γ , as it makes x independent of the expansion of the Universe after electron-positron annihilation, with both $T, \nu \propto (1+z)$. The electron temperature on the other hand evolves in a non-trivial way after baryons thermally decouple from radiation at $z \sim 500$. The total y_γ parameter for an energy injection redshift of z_{inj} is then given by $y_\gamma(z_{\text{inj}}) \equiv y_\gamma(0, z_{\text{inj}})$. The Compton parameter $y_\gamma(z_{\text{inj}})$ is plotted in Fig. 4 and it can be seen that the contribution to the integral from $z < 1.5 \times 10^4$ becomes very small, with $y_\gamma \lesssim 0.01$. We will present our results as functions of y_γ and they can be converted into functions of redshifts using Eq. 4.1 and Fig. 4. During radiation domination, we can calculate the y_γ parameter analytically and is given by $y_\gamma(z, z_{\max}) \approx \frac{k_B \sigma_T}{m_e c} \frac{(n_H + 2n_{\text{He}}) T_{\text{CMB}}}{2H_0 \Omega_r^{1/2}} \left[(1+z_{\max})^2 - (1+z)^2 \right] = 4.88 \times 10^{-11} \left[(1+z_{\max})^2 - (1+z)^2 \right]$, where n_H and n_{He} are the number densities of hydrogen and helium nuclei today respectively, and Ω_r is the radiation energy density today in units of critical density. Similarly, it is easy to find analytic formulae during the matter dominated era, $z \ll 3200$, but before recombination and also after reionization, when the electron density is again simply equal to sum of hydrogen and helium number densities (assuming singly ionized helium).

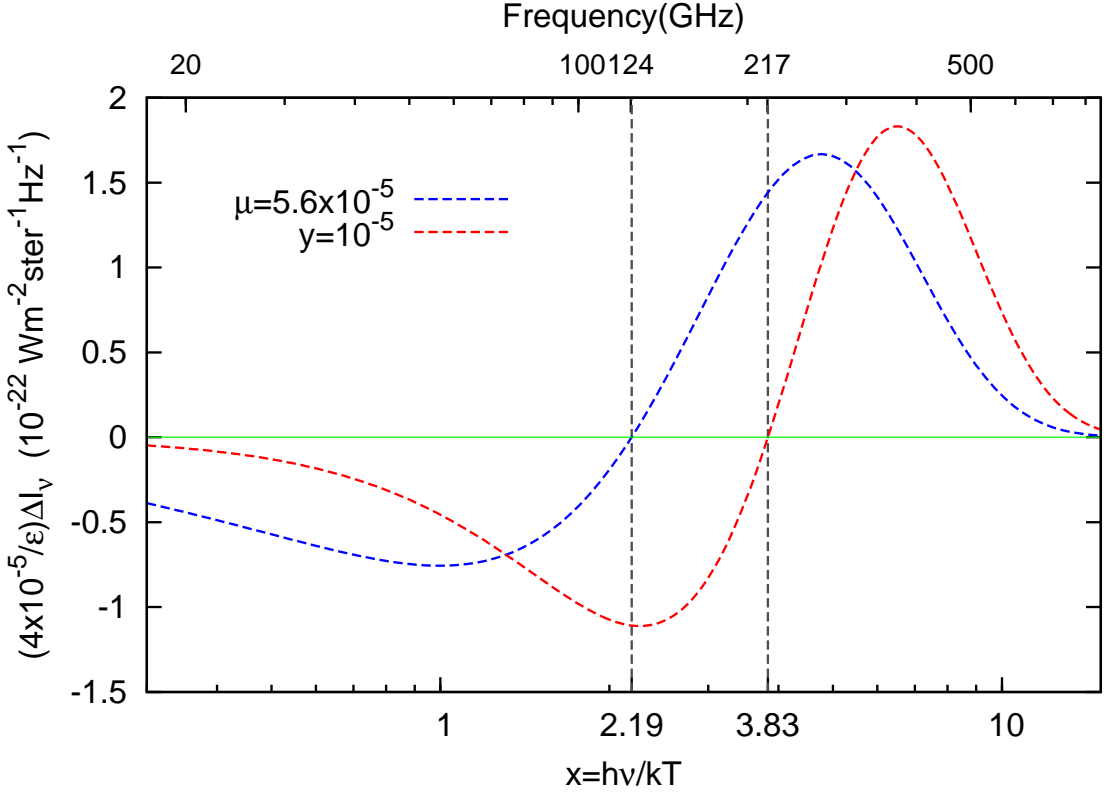


Figure 3. Same as Fig. 2 but difference in intensity from a blackbody with reference temperature T is plotted.

We also define the Compton y -type distortion amplitude, y ,

$$\begin{aligned}
 y &= \int_0^{y_\gamma} \Delta_{T_e} dy_\gamma \equiv - \int_{z_{\max}}^z \frac{k_B \sigma_T}{m_e c} \frac{n_e (T_e - T)}{H(1+z)} dz \\
 &\approx_{T_e \gg T} - \int_{z_{\max}}^z \frac{k_B \sigma_T}{m_e c} \frac{n_e T_e}{H(1+z)} dz \equiv y_e,
 \end{aligned} \tag{4.2}$$

where, $\Delta_{T_e} \equiv T_e/T - 1$, and T_e is the electron temperature. The last line gives the familiar result in terms of electron pressure relevant for hot electrons, for example, in the clusters of galaxies. The Compton parameter y_γ is a measure of the degree of comptonization including the effect of all three relevant processes: recoil, induced recoil and Doppler broadening (the latter determined by $y_\gamma T_e/T$). The distortion amplitude y on the other hand is a measure of the amount of heating (or cooling). As an example, we show in Fig. 5 the expected post-recombination rate of thermal y -distortion injection into the CMB. Before reionization, we get negative y -type distortions due to comptonization with colder electrons which cool much faster with the expansion of the Universe [12] and can be identified as Bose-Einstein condensation [15]. Reionization, in addition to increasing ionization, also heats up the intergalactic medium. We have assumed $T_e = 10^6/(1+z)^{3.3}$ K at $z < 3$ taking into account the contributions from the warm hot intergalactic medium (WHIM) [51, 52] and 10^4 K at $z > 3$. Total y -type distortion from reionization is $y_\gamma \Delta_{T_e} \sim (k_B T_e/m_e c^2) \tau_{ri} \sim 10^{-6} \times 0.1 = 10^{-7}$ while from WHIM at smaller redshifts, it is expected to be $\sim 10^{-6}$ [53–56]. These y -type distortions should be detectable by PIXIE [5] while the proposed experiment Cosmic Origins Explorer (CORe) [57] with similar resolution but significantly higher sensitivity than PLANCK spacecraft [58] and ground based

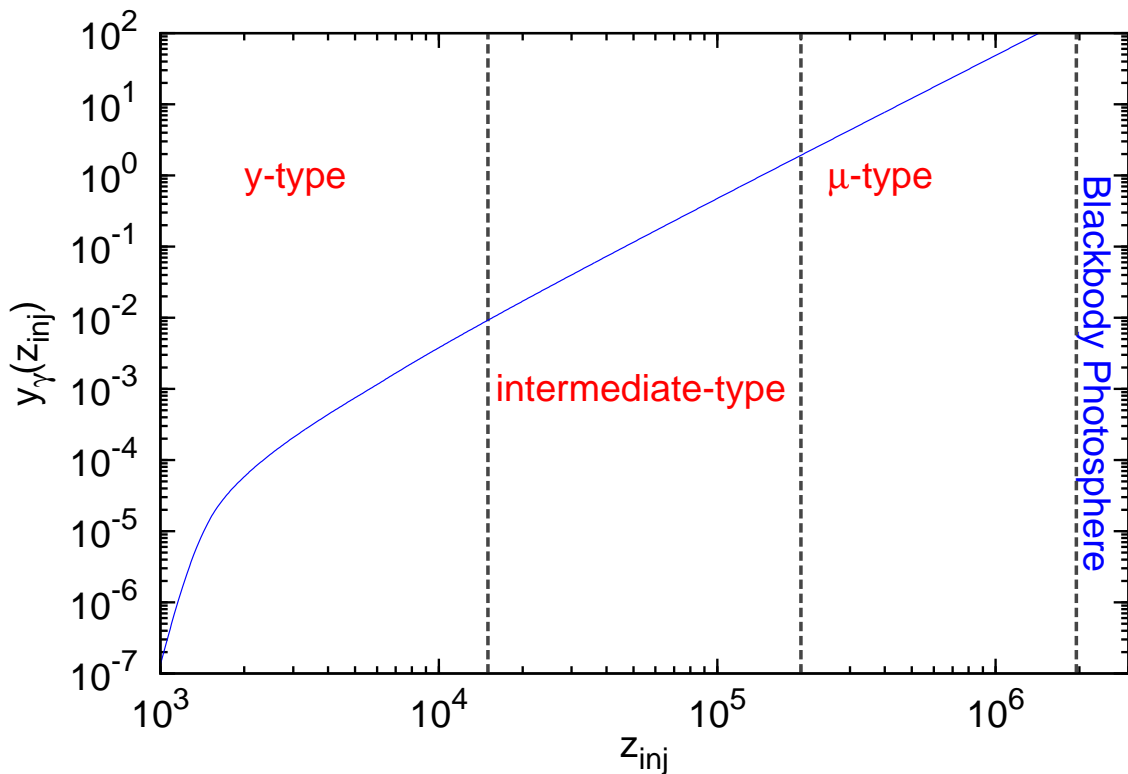


Figure 4. Dependence of Compton parameter on redshift, $y_\gamma(z_{\text{inj}}) = - \int_{z_{\text{inj}}}^0 dz [k_B \sigma_T n_e T] / [m_e c H (1+z)]$. The drop in the plot at $z \sim 1000$ is due to the depletion of electrons because of recombination. The total energy released is divided approximately equally between y -type, intermediate-type and μ -type distortions for the case of Silk damping with spectral index of initial power spectrum close to unity [e.g. see 15] and for other mechanisms with similar rate of energy injection, e.g. dark matter annihilation. For energy release from exponential decay of particles, the division of energy is less democratic and depends sensitively on the lifetime of the particle. Recombination [45–47] was calculated using the effective multilevel approach [48] following publicly available codes HyRec [49] and CosmoRec [50].

experiments ACTPol [59] and SPTPol [60] should also be able to detect y -fluctuations in the WHIM. We have also assumed that reionization starts at $z \sim 20$ and ends at $z \sim 8$. Uncertainties in the details of reionization and temperature evolution of the intergalactic medium make it impossible, at least at present, to disentangle the pre-recombination and post-recombination contributions to the y -type distortions. There will also be contributions from the second order Doppler effect from baryon peculiar velocities [61, 62], not shown in the figure, before during and after reionization. These contributions during and after recombination are calculated in [13].

With the above definitions, we can now use the standard form of Kompaneets equation [20] (taking care to distinguish between the actual electron/effective photon temperature T_e and the blackbody temperature T used to define the variable x):

$$\frac{\partial n}{\partial y_\gamma} = \frac{1}{x^2} \frac{\partial}{\partial x} x^4 \left(n + n^2 + \frac{T_e}{T} \frac{\partial n}{\partial x} \right). \quad (4.3)$$

The first term in the parenthesis describes the downward scattering of photons due to electron recoil, second term is for induced scattering while the last term describes diffusion of photons in energy due

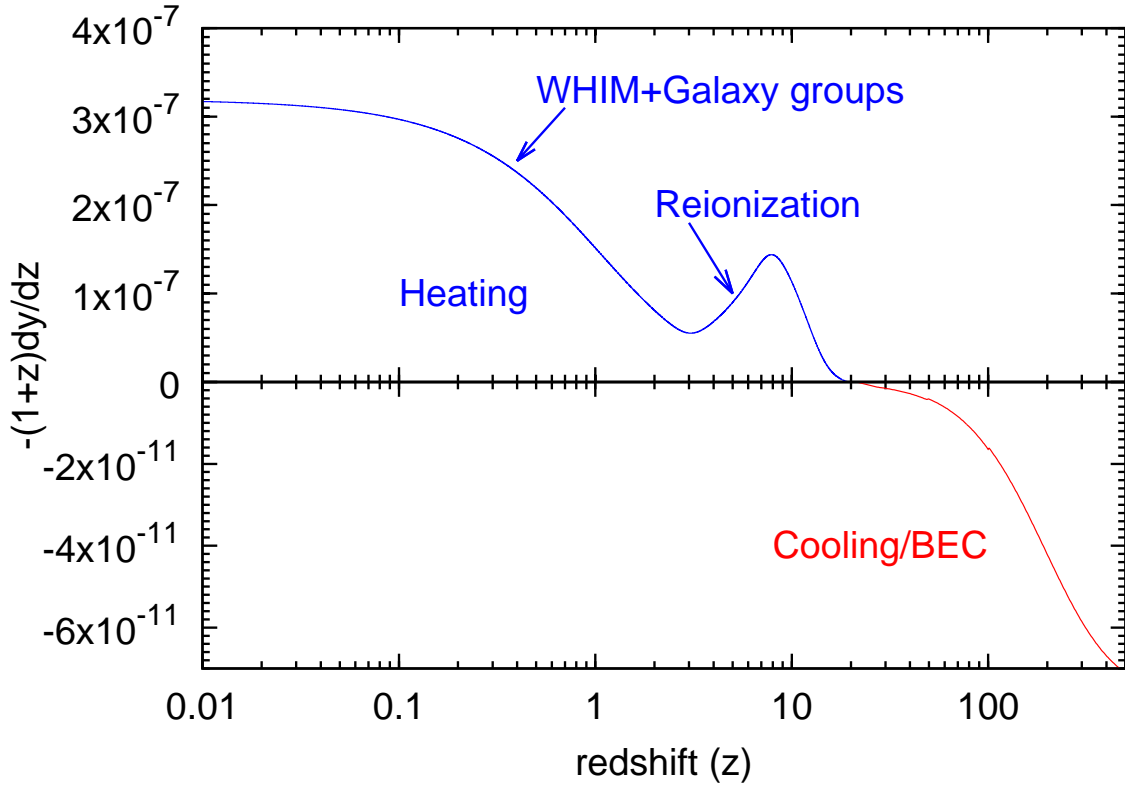


Figure 5. Post-recombination (rough) estimate of the thermal y -distortion injection rate $-(1+z)dy/dz$ is plotted, it is approximately equivalent to the energy release in the redshift interval $\delta z \sim z$. Before reionization starts, the distortions are dominated by cooling of CMB or Bose-Einstein condensation (BEC) due to comptonization with colder electrons giving a negative y distortion. During and after reionization the intergalactic medium is heated to temperature $T_e \gtrsim 10^4$ giving a much larger positive y distortion of amplitude $\sim 10^{-7}$. There will also be similar magnitude positive contributions from the second order Doppler effect (not shown above) arising due to peculiar velocities of electrons.

to Doppler effect and thus depends on the electron temperature. At high frequencies $n \ll 1$ and the induced scattering term can be neglected. If a source of energy raises the electron temperature such that $T_e \gg T$ for a very short time, $y_\gamma \ll 1$, an analytical solution, for the initial condition $n(x, y_\gamma = 0) = n_{\text{pl}}(T)$ (blackbody spectrum at temperature T), of the Kompaneets equation can be obtained by approximating the recoil terms $n + n^2$ with the initial blackbody spectrum $n_{\text{pl}} + n_{\text{pl}}^2$. The fact that the Planck (and in general Bose-Einstein) spectrum is an equilibrium solution of the Kompaneets equation ([20],[63],[44]) gives $n + n^2 \approx -dn/dx$. The resulting equation can be transformed into heat diffusion equation, the analytic solution of which is the well known y -type distortion [3], Eq. (3.4). We derive these results in Appendix B in a way which clearly illustrates the regime of validity of the solution.

5 Evolution of y -type distortion

We will now consider the problem of comptonization of an initial y -type distortion created by an energy source which turned on for a very short time, i.e., instantaneous energy injection. This problem will illustrate the main physics we want to investigate. We will explore the more realistic cases of

continuous energy injection in the next sections. However, it is possible that such short lived sources may actually exist. In fact, one such example can be found in standard cosmology. The decay of primordial ${}^7\text{Be}$ to ${}^7\text{Li}$ lasts for a very short time at $z \sim 30000$ [64] and gives rise to exactly the type of distortions we calculate in this section (although energy released in Be decay is too small to be of observational interest). The spectrum we get from ${}^7\text{Be}$ is the $y_\gamma = 0.04$ spectrum and is given approximately by Eq. (5.3) with $y \sim 10^{-16}$.

The y -type spectrum should evolve towards the Bose-Einstein equilibrium solution with time. The equilibrium electron temperature or effective photon temperature T_e is given by [65, 66]

$$\frac{T_e}{T} = \frac{\int (n + n^2)x^4 dx}{4 \int nx^3 dx} \quad (5.1)$$

The effective temperature for the linear y -type spectrum for energy injection $\Delta E/E$ is given by [44] $T_e = T(1 + 5.4y) = T(1 + 1.35\Delta E/E)$. The exact temperature will be slightly higher if y is not small. For a Bose-Einstein spectrum the effective temperature is $T_e \approx T(1 + 0.456\mu) \approx T(1 + 0.64\Delta E/E)$. This temperature is established very fast compared to any other relevant process with a characteristic time of ~ 1 s at $z = 10^5$, ~ 10 orders of magnitude faster than the expansion rate of the Universe at that time. The electrons will thus always be maintained at the effective photon temperature given by Eq. 5.1. As the y -type spectrum evolves towards the Bose-Einstein spectrum, the electron temperature should decrease.

5.1 Numerical solution in the intermediate era, $1.5 \times 10^4 \lesssim z \lesssim 2 \times 10^5$

To follow the evolution of the spectral distortions starting with the y -type distortion, we must solve Eq. 5.1 and Kompaneets equation Eq. 4.3 simultaneously. Numerically we proceed as follows. We take small steps in time y_γ using Kompaneets equation with constant T_e given by Eq. 5.1 for the spectrum at the beginning of the step. We then calculate the final electron temperature using Eq. 5.1 and iterate, with T_e linearly decreasing between the initial and final values. We found that a step size of $\delta y_\gamma = 0.001$ at $y_\gamma < 1$ and $\delta y_\gamma = 0.01$ at $y_\gamma > 1$ was sufficiently accurate. With our iterative procedure the error in energy conservation is $< 1\%$ at $y_\gamma < 10$. Fig. 6 show the cooling of the photon spectrum as the Bose-Einstein distribution is approached. Initially the temperature drops rapidly from the y -type value of $\Delta T_e/T = 5.4y$ and is close to the linear Bose-Einstein value of $2.56y$ at $y_\gamma = 1$. Fig. 6 shows that for small distortions, $\Delta n/n \ll 1$ and $|(T_e - T)/T| \ll 1$, the equilibrium Bose-Einstein spectrum is reached at $y_\gamma \gg 1$ and the spectrum is very close to the equilibrium at $y_\gamma \sim 1$. This conclusion does not depend on the amplitude of the distortion, y , at all because the processes responsible for comptonization, Doppler broadening and recoil, are defined by the parameters $y_\gamma T_e/T$ and y_γ respectively.

Difference in observed intensity from a blackbody is shown in Fig. 7 and Fig. 8 shows the fractional difference in the effective temperature with respect to T as the photon distribution moves from the y -type spectrum towards the Bose-Einstein spectrum. An interesting feature is that the zero point, defined as x_0 such that $n(x_0) = n_{\text{pl}}(x_0)$, moves from the y -type distortion value of $x_0 = 3.83$ to Bose-Einstein value of $x_0 = 2.19$. The maxima and minima of the intensity distortion also move towards smaller frequencies as comptonization progresses. Zero point x_0 is plotted in Fig. 9. Frequencies of maxima and minima, $x_{\text{min}}, x_{\text{max}}$ are also plotted in Fig. 9 and the corresponding intensities, $\Delta I_{\text{min}}, \Delta I_{\text{max}}$ in Fig. 10. The Bose-Einstein spectrum at $x > 10$ is in fact established very quickly. By $y_\gamma = 0.2$ the spectrum is very close to the Bose-Einstein spectrum corresponding to the electron temperature $T_e(y_\gamma)$ at $x > 10$. At $y_\gamma > 0.2$, the spectrum at high x remains Bose-Einstein and tracks the electron temperature as the effective radiation/electron temperature decreases. Fitting formulae for $x_0, x_{\text{min}}, x_{\text{max}}$ are given in Appendix A.

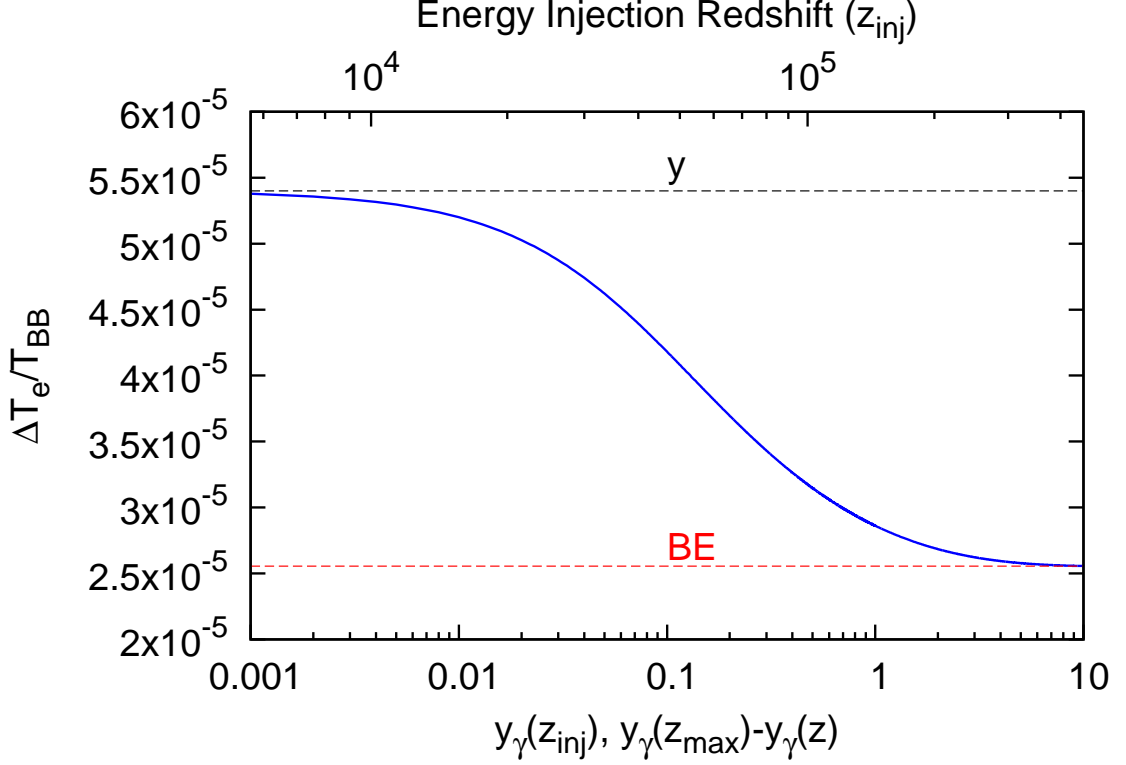


Figure 6. Evolution of electron temperature for initial spectrum with $y = 10^{-5}$. Initial fractional difference in temperature $\Delta T_e/T \equiv (T_e - T)/T = 5.4 \times 10^{-5}$. The final temperature for the Bose-Einstein spectrum is also marked at $\Delta T_e/T = 2.56 \times 10^{-5}$. By $y_\gamma = 0.01$ the temperature is significantly different from the initial temperature and by $y_\gamma = 2$ it is very close to the Bose-Einstein spectrum temperature. This and subsequent plots in this section can be interpreted as snapshots in the evolution of initial y -spectrum starting from initial energy injection redshift z_{\max} to redshift z , so that the x-axis is $y_\gamma = y_\gamma(z_{\max}) - y_\gamma(z)$. Alternatively, it can be interpreted as the final spectrum today resulting from the energy injection at redshift z_{inj} , so that $y_\gamma = y_\gamma(z_{\text{inj}})$.

5.2 Analytic solution in the weak comptonization limit

We can find an analytic solution for the evolution of an initial y -type distortion by expanding $n(x, y_\gamma)$ around $y_\gamma = 0$, using the Taylor series expansion, Eq. (B.1). The initial spectrum is the y -type spectrum with amplitude y , $n(x, 0) = n_{\text{pl}}(x) + y n_y(x)$, and the initial electron temperature is given by the equilibrium temperature, Eq. (5.1), $\Delta T_e \approx 5.4y$. Substituting the initial spectrum in the Kompaneets equation gives us the first term in the Taylor series (assuming $y \ll 1$ and only keeping terms linear in y),

$$\begin{aligned} \frac{\partial n}{\partial y_\gamma}(x, 0) &= \frac{1}{x^2} \frac{\partial}{\partial x} \left[x^4 \left(\frac{\partial n(x, 0)}{\partial x} \left(\frac{T_e}{T} \right) + n(x, 0) + n(x, 0)^2 \right) \right] \\ &\approx \Delta T_e n_y(x) + y f_y(x), \end{aligned} \quad (5.2)$$

where $n_y(x)$ is the y -type spectrum defined in Eq. (3.4), and $f_y(x)$ is the same function which appeared in Eq. (B.3) and is given in the appendix, Eq. (C.1). We thus have the solution for the weakly

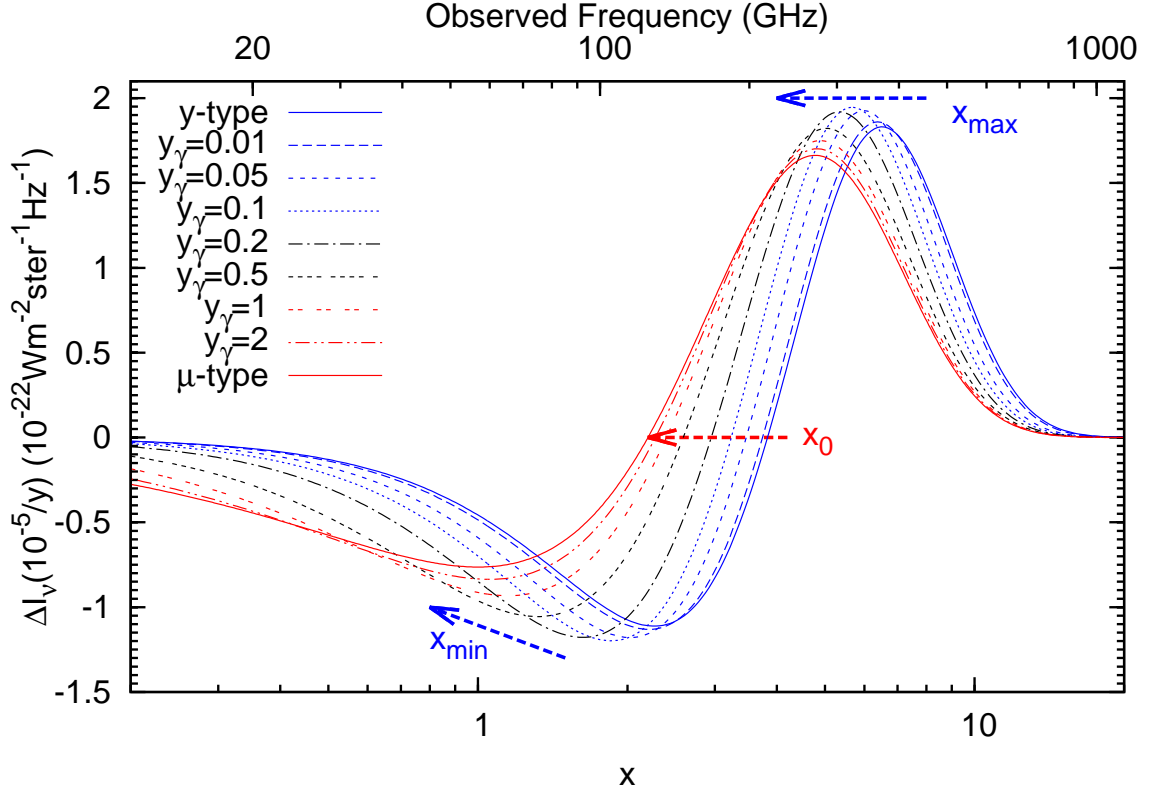


Figure 7. Intermediate-type spectra: Difference in intensity from a blackbody at temperature T is plotted. Bose-Einstein and y -type spectra for same value of energy injection are also shown. Initial spectrum is a pure y -type distortion (Eq. (3.4) with $y = 10^{-5}$) and is labeled $y_\gamma = 0$. The curves in order of increasing (non zero) y_γ correspond to energy injection redshift of $z_{inj} = 1.56 \times 10^4, 3.33 \times 10^4, 4.67 \times 10^4, 6.55 \times 10^4, 1.03 \times 10^5, 1.45 \times 10^5, 2.04 \times 10^5$. The 'zero' point, the frequency x where the intensity equals that of blackbody at temperature T moves from the y -type distortion value of 3.83 to Bose-Einstein value of 2.19.

comptonized spectrum,

$$\begin{aligned}
 n(x, y_\gamma) &\approx n_{pl}(x) + y \left[n_y(x) + y_\gamma (5.4 n_y(x) + f_y(x)) \right] \\
 &= n_{pl}(x) + y n_y(x) \left[1 + y_\gamma \left(5.4 + \frac{f_y(x)}{n_y(x)} \right) \right],
 \end{aligned} \tag{5.3}$$

where we have the following simplified expression and large x and small x limits,

$$\begin{aligned}
 \frac{f_y(x)}{n_y(x)} &= \frac{8}{x \coth\left(\frac{x}{2}\right) - 4} + x [x - \sinh(x)] \operatorname{csch}^2\left(\frac{x}{2}\right) + 6 \\
 &\xrightarrow{x \gg 1} -2x, \\
 &\xrightarrow{x \ll 1} 2
 \end{aligned} \tag{5.4}$$

The correction $f_y(x)$, of course, similarly to $n_y(x)$, conserves photon number, $\int_0^\infty dx f_y(x) x^2 = 0$.

The next terms in the Taylor series can be calculated iteratively by taking successive y_γ -derivatives of Kompaneets equation. We give the recursion relations to calculate any higher order term in

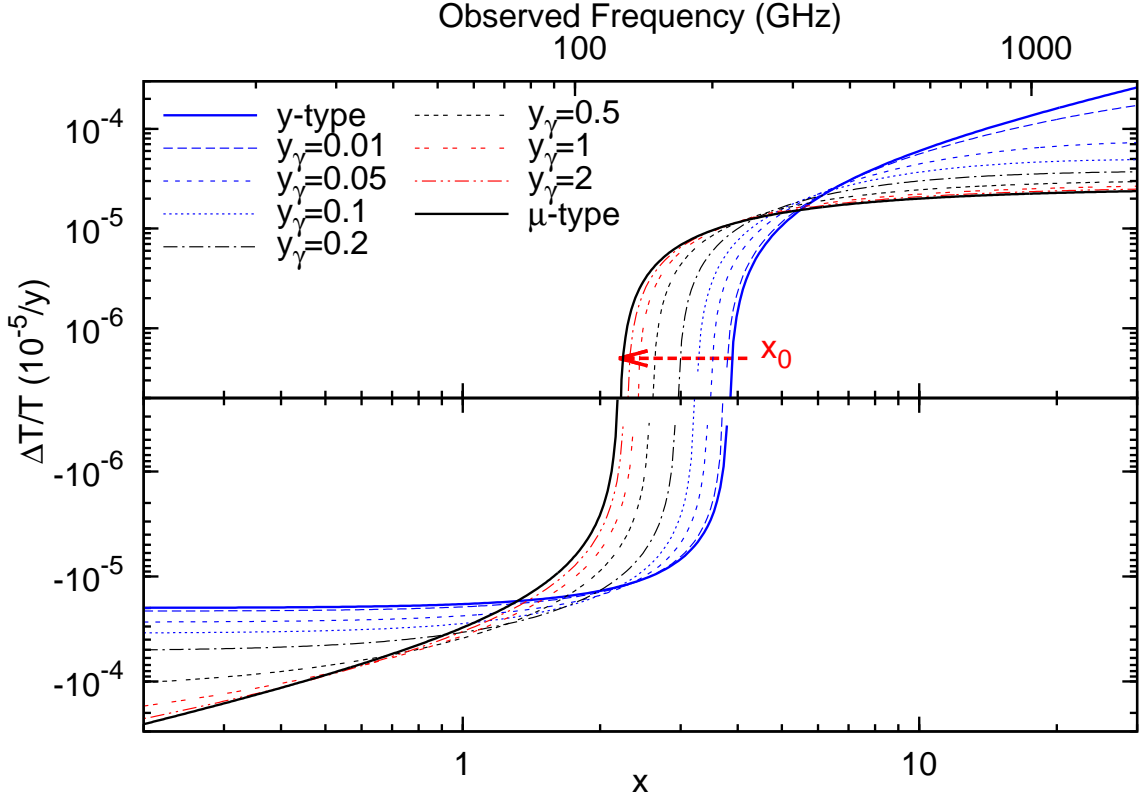


Figure 8. Intermediate-type spectra: Fractional difference $\frac{\Delta T}{T} \approx \frac{1-e^{-x}}{x} \frac{\Delta n}{n_{\text{pl}}}$ in effective temperature (Eq. (3.5)) is plotted. Bose-Einstein spectrum for same value of energy injection is also shown. Initial spectrum is a pure y -type distortion (Eq. (3.4) with $y = 10^{-5}$) and is labeled $y_\gamma = 0$. The curves in order of increasing (non zero) y_γ correspond to energy injection redshift of $z_{\text{inj}} = 1.56 \times 10^4, 3.33 \times 10^4, 4.67 \times 10^4, 6.55 \times 10^4, 1.03 \times 10^5, 1.45 \times 10^5, 2.04 \times 10^5$. The 'zero' point, maxima and minima of the frequency move towards smaller frequencies as comptonization progresses.

Appendix C. The y_γ -derivatives of the electron temperature are also required and are easily calculated using Eq. (5.1). The first two derivatives are given by, $d\Delta T_e/dy_\gamma|_{y_\gamma=0} \approx -21.45y$, and $d^2\Delta T_e/dy_\gamma^2|_{y_\gamma=0} \approx 323.6y$. Intermediate distortions for case of continuous energy release, for example particle decay/annihilation, Silk damping, are easily obtained from these analytic formulae by linearly adding (integrating) the spectra for different y_γ with appropriate weights. Analytic solution including first three terms are quite precise ($\sim 1\%$ error) for $y_\gamma \lesssim 0.05$ deteriorating to $\sim 10\%$ errors at $y_\gamma = 0.1$. Numerical and analytic solutions are compared in detail in Appendix C.

6 Application: Amplitude, slope and shape of the primordial power spectrum on small scales

The solutions given in the previous section would be directly applicable if the energy injection occurs over a very short period of time. It is more likely, in reality, that the energy release happens over an extended period of time, for example, decay of particles or dissipation of sound waves. The final spectrum for continuous energy injection would be a superposition of spectra for all values of y_γ parameter, with appropriate weights decided by the dependence of rate of energy injection on redshift, and we must calculate the spectrum for each model of energy release numerically. The shape

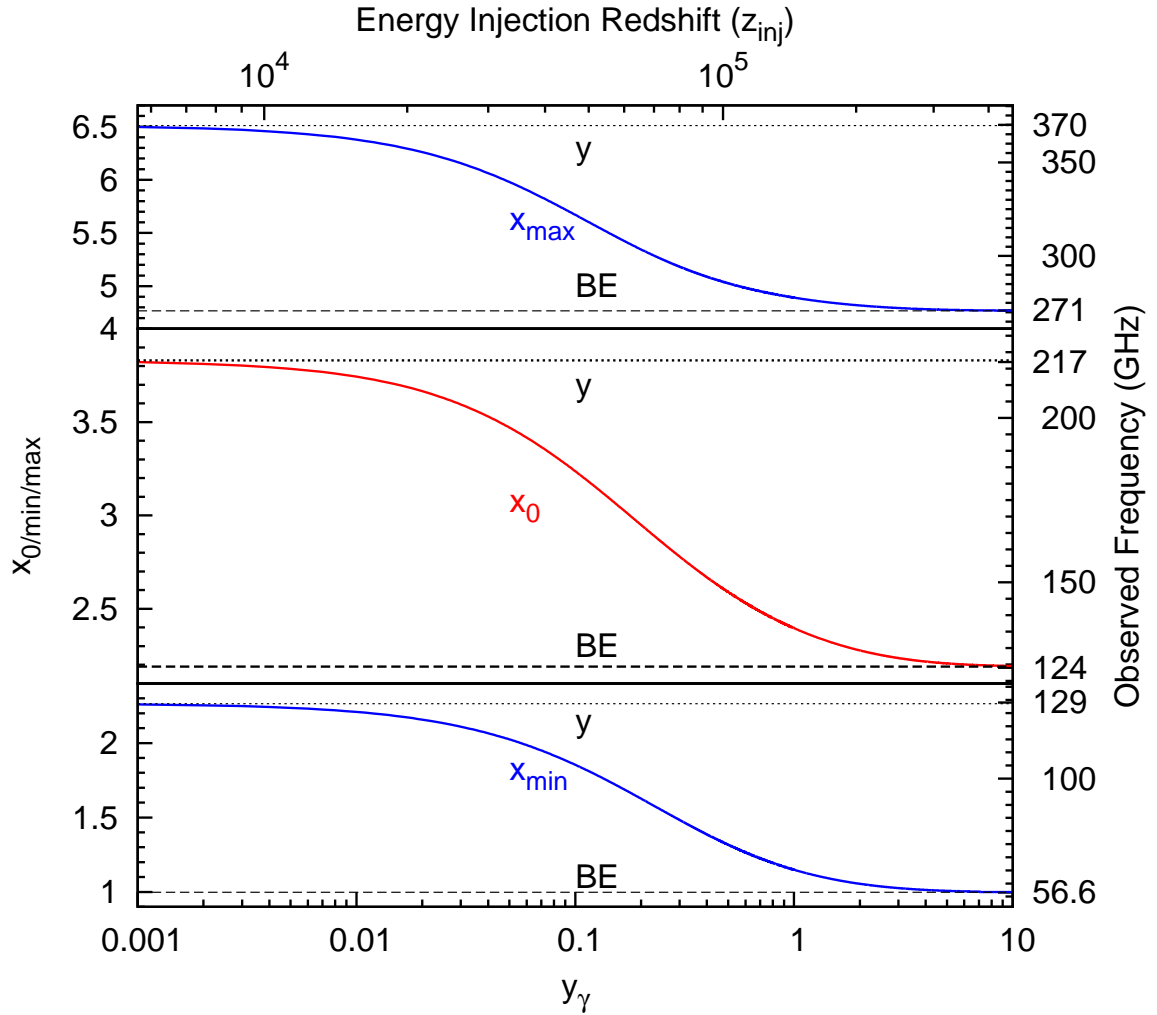


Figure 9. Evolution of the zero point x_0 defined by $n(x_0) = n_{\text{pl}}(x_0)$, and frequency of minima and maxima of the intensity of distortion, x_{min} and x_{max} . x_0 can be used to pinpoint the redshift of energy injection in case a distortion in CMB spectrum is detected.

of the power spectrum and the value of x_0 will still contain information about the energy release as a function of time, in addition to the total amount of energy released. This is in contrast to the pure μ -type (or y -type) distortion which only contains information about the total energy injected.

One of the most important sources of heating in standard cosmology is the dissipation of sound waves in the early Universe because of the shear viscosity (and at late times also due to thermal conduction) on small scales. The dissipation of sound waves resulting from thermal conduction was first calculated by Silk [8], Peebles and Yu [71] included shear viscosity and Kaiser [72] included the effect of photon polarization. The spectral distortions arising from the dissipation of sound waves have also been studied by many authors in the past using approximate estimates [9–11] and a precise calculation was done recently by [13]. Primordial perturbations excite standing sound waves in the early Universe on scales smaller than the sound horizon [73–75]. Diffusion of photons from different phases of the waves, of wavelength of the order of diffusion length, gives rise to a local quadrupole which is isotropized by Thomson scattering (shear viscosity). The effect on the photon spectrum is

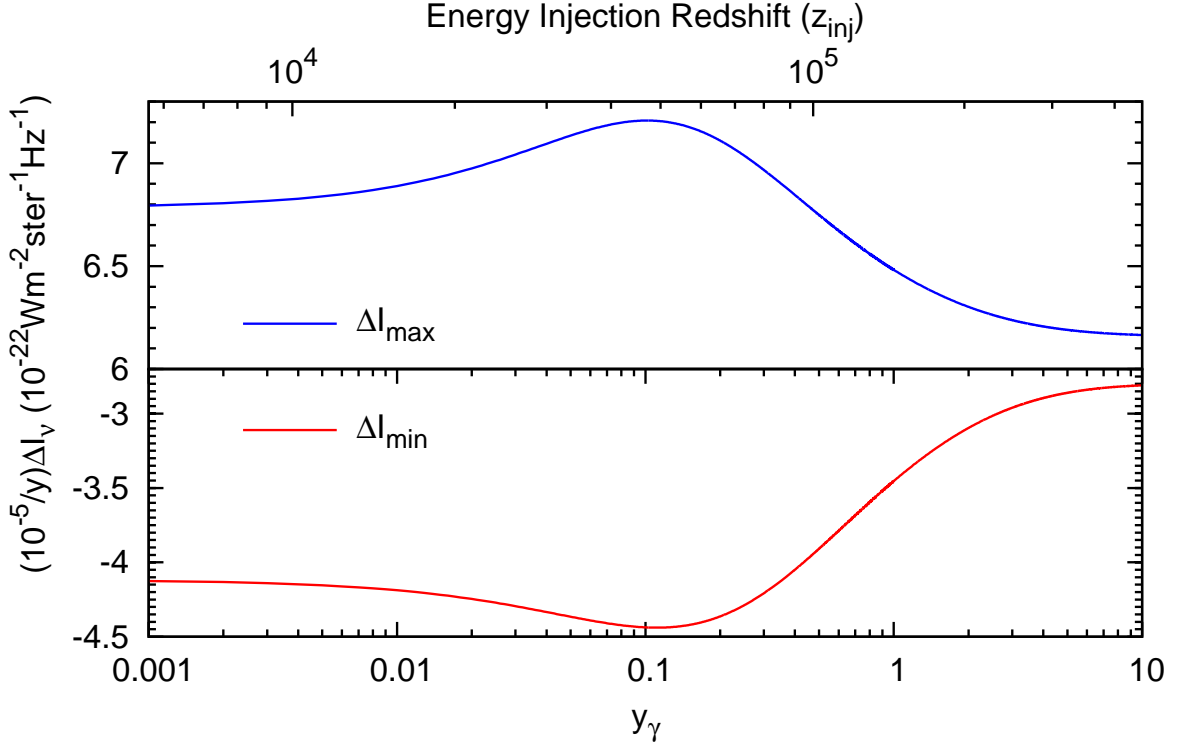


Figure 10. Minimum and Maximum of the intensity of distortion from the reference blackbody, ΔI_ν

just the averaging of the blackbodies of different temperature and gives rise to y -type distortions [76]. The y -type distortions can then Comptonize, fully or partially, giving rise to a μ -type distortion or an intermediate-type spectrum [9, 11]. We should also mention that the adiabatic cooling of baryons due to the expansion of the Universe gives spectral distortions of an amplitude opposite to those given by heating [12]. We include this cooling of baryons (or equivalently small difference of electron temperature from the effective photon temperature given by Eq. (5.1)) in our calculations; this is, however, a very small correction to the amount of heating considered below. Also, the low frequency spectrum is affected by bremsstrahlung emission/absorption after recombination [12]. In the frequency range of interest to us, $\nu \gtrsim 30$ GHz, $x \gtrsim 0.5$ and for distortions of interest, with amplitude $\Delta E/E \gtrsim 10^{-9}$, low redshift bremsstrahlung (and double Compton scattering) can be neglected.

The precise total spectrum resulting from sound wave dissipation was calculated recently by [13] including contributions from the μ -type era, intermediate era and the y -type era. Here we consider the possibility that the pure μ -type distortions created at $y_\gamma > y_{\gamma_{\max}} = 2 (z \gtrsim 2 \times 10^5)$ and pure y -type distortions created at $y_\gamma < y_{\gamma_{\min}} = 0.01 (z \lesssim 1.6 \times 10^4)$ can be subtracted with high precision (see Fig. 7). The exact upper/lower limits (and the resulting intermediate spectrum) will of course depend on the ability of the experiment to distinguish a pure μ -type (y -type) from a $y_{\gamma_{\max}}$ ($y_{\gamma_{\min}}$) intermediate-type spectrum. The heating rate due to an initial power spectrum with constant scalar index on small-scales n_{ss} is given by [13, 43]

$$\frac{d\mathcal{E}}{dz} = \frac{3.25 A_\zeta}{k_0^{n_{\text{ss}}-1}} \frac{d(1/k_D^2)}{dz} 2^{-(3+n_{\text{ss}})/2} k_D^{n_{\text{ss}}+1} \Gamma\left(\frac{n_{\text{ss}}+1}{2}\right), \quad (6.1)$$

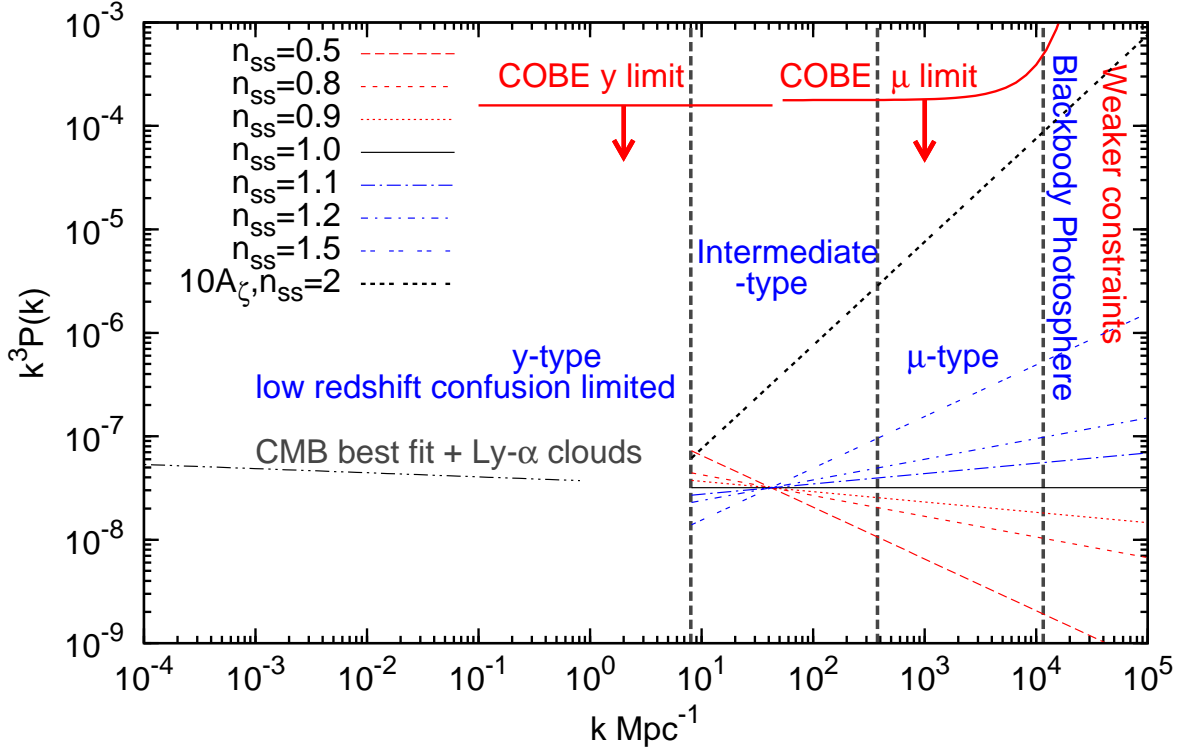


Figure 11. The power spectra, Eq. (6.3), with different indices n_{ss} on small scales are shown, for constant amplitude. Also shown for reference is the best-fit WMAP power spectrum on large scales with $n_s = 0.96$ [33, 67, 68] with Ly- α forest extending the constraints to smaller scales [69, 70]. The small scale limits on power from COBE/FIRAS measurements of CMB spectral distortions are also shown. There is considerable freedom in varying the amplitude and the spectral index of the power spectrum within COBE/FIRAS limits. We show this by the curve with 10 times the amplitude and extreme value for the spectral index $n_{ss} = 2$. PIXIE [5] is expected to improve COBE/FIRAS constraints by a factor of $\sim 2.5 \times 10^3$.

where $\mathcal{E} = E/\rho_\gamma$, E is the total energy in photons and $\rho_\gamma = a_R T_{\text{CMB}}^4 (1+z)^4$ is the reference photon energy density, a_R is the radiation constant, $T_{\text{CMB}} = 2.725$ K is the CMB temperature today, k_D is the damping wavenumber given by [72, 77]

$$\frac{1}{k_D^2} = \int_z^\infty dz \frac{c(1+z)}{6H(1+R)n_e\sigma_T} \left(\frac{R^2}{1+R} + \frac{16}{15} \right) \quad (6.2)$$

where $R \equiv 3\rho_b/4\rho_\gamma$, ρ_b is the baryon energy density. We have defined the power spectrum of initial curvature perturbation in comoving gauge ζ as

$$P_\zeta = A_\zeta \frac{2\pi^2}{k^3} \left(\frac{k}{k_0} \right)^{n_{ss}-1}. \quad (6.3)$$

An important point to note here is that for $n_{ss} = 1$, the energy released between redshifts z_1 and z_2 is proportional to $\ln[(1+z_1)/(1+z_2)]$ [15] and it is easily seen that the total energy released at $z \gtrsim 1000$ is divided approximately equally between y , μ and intermediate-type distortions. For smaller spectral index $n_{ss} < 1$, intermediate-type distortions get bigger and bigger share of the total energy released

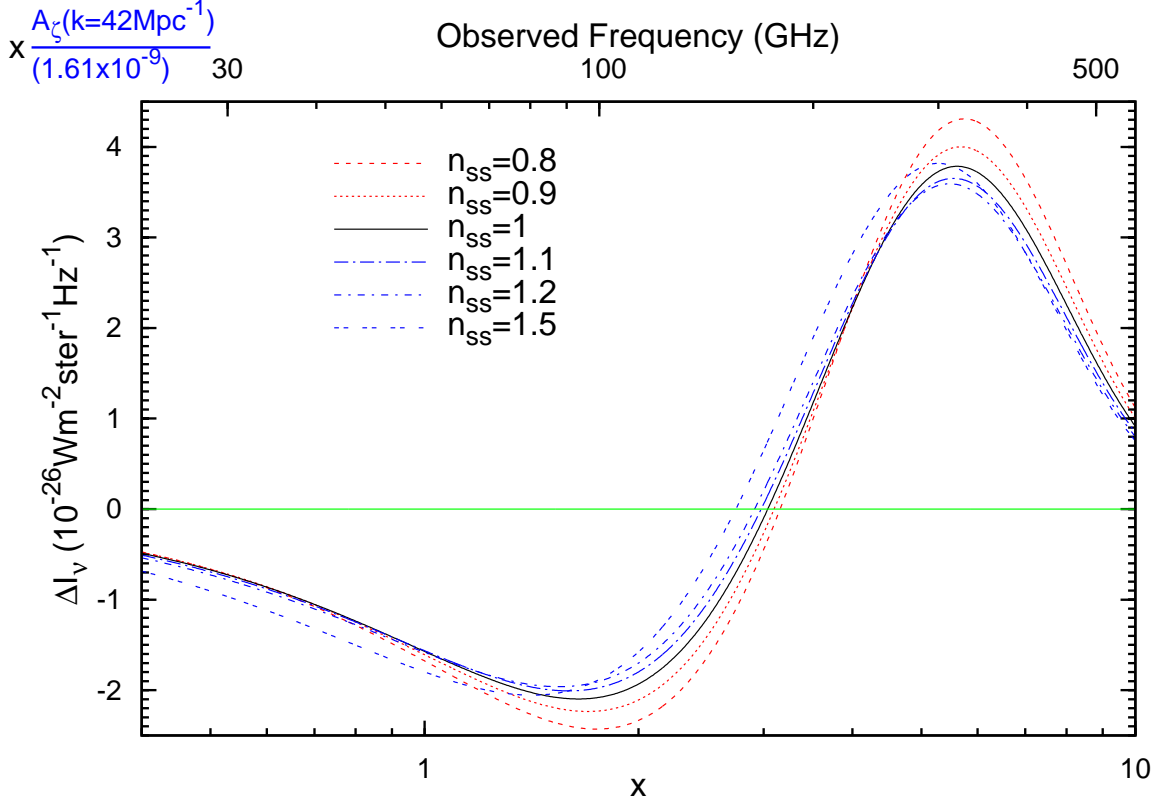


Figure 12. Distortion spectrum created by dissipation of sound waves in the redshift range $1.56 \times 10^4 \leq z \leq 2.04 \times 10^5$ corresponding to the y_γ parameter $0.01 \leq y_\gamma \leq 2$. Difference in intensity from the reference blackbody spectrum with the same number density of photons is plotted. Different plots are for different values of small scale spectral index n_{ss} of the initial power spectrum normalized so that they all have the same power at the pivot point $k = 42 \text{ Mpc}^{-1}$ as the WMAP best fit power spectrum with $n_s = 0.96$, which is the value of diffusion wavenumber k_D at $y_\gamma = 0.1, z = 4.67 \times 10^4$. These are the distortions that would be left over after pure y_γ and μ type distortions are subtracted and probe *shape* as well as the amplitude of the small scale power spectrum in the range $8 \lesssim (k \sim k_D) \lesssim 378 \text{ Mpc}^{-1}$.

with y -type distortions comparatively enhanced and μ -type distortions comparatively suppressed. The exact opposite, of course, happens for larger spectral indices $n_{ss} > 1$.

Since we want to compare the shape of spectral distortions for different power spectra with similar total energy input, we choose the pivot point $k_0 = k_D(y_\gamma = 0.1, z = 4.67 \times 10^4) = 42 \text{ Mpc}^{-1}$ corresponding to the approximate (geometric) middle of our redshift range for intermediate-type spectral distortions. We choose the amplitude $A_\zeta = 1.61 \times 10^{-9}$ to match the power at $k = 42 \text{ Mpc}^{-1}$ with the WMAP best fit power spectrum with $n_s = 0.96$ [33]. The spectral index, n_{ss} , on small scales, $k \gtrsim 8 \text{ Mpc}^{-1}$ can be very different from the spectral index on large scales, n_s , measured by WMAP, for example, in the case of a running spectrum. The small-scale power spectra, with different indices n_{ss} , are shown in Fig. 11. CMB constrains the primordial power spectrum only on large scales [33, 67, 68], $k \lesssim 0.2 \text{ Mpc}^{-1}$. This range can be extended to $\sim 1 \text{ Mpc}^{-1}$ using Ly- α forest [69] and is consistent with the WMAP best fit power spectrum parameters [70]. The small scales are best constrained by COBE/FIRAS data through limits on y and μ -type distortions [1]. We have shown these constraints, assuming $n_{ss} = 1$ and using the fitting formulae in [13] to calculate the y and μ type distortions. These constraints are more than 3 orders of magnitude higher than a simple extrapolation

of the WMAP best fit power spectrum to small scales. Thus, there is considerable freedom, from an observational viewpoint, for the power spectrum on the small scales to be quite different from the extrapolation of the WMAP power spectrum to these scales. The constraints get considerably weaker behind the blackbody surface at small scales, $k \gtrsim k_D(z = 2 \times 10^6) = 1.15 \times 10^4 \text{ Mpc}^{-1}$, because of the suppression of the μ distortion by blackbody visibility function [2]. The visibility function is dominated by the double Compton process in a low baryon density Universe such as ours [6] and is given by $\approx \exp[-(z/2 \times 10^6)^{5/2}]$.³ We sketch this weakening of the constraints by multiplying the COBE/FIRAS constraint by the inverse of the visibility function $\exp[(k/1.15 \times 10^4 \text{ Mpc}^{-1})^{5/3}]$, using $k_D \propto (1+z)^{3/2}$. The μ -type distortion, of course, only provide integrated constraints on the total energy injected in the μ -distortion and its separation into individual contributions from different epochs is not possible in practice.

To calculate the spectrum arising from a continuous source of heating, such as dissipation of sound waves, we should solve the Kompaneets equation Eq. (4.3) with a source term on the right hand side given by

$$\left. \frac{dn}{dy_\gamma} \right|_{\text{source}} = \frac{1}{4} \frac{d\mathcal{E}}{dz} \frac{dz}{dy_\gamma} n_y, \quad (6.4)$$

where n_y is the y -type distortion given by Eq. (3.4) which is created initially and the factor of $1/4$ comes from the relation between the energy injected and the amplitude y of the y -type distortion. We show the intermediate-type spectrum resulting from the dissipation of sound waves for several different values of the small scale spectral index $0.5 < n_{ss} < 1.5$ in Figs. 12 (intensity). The amplitude of the distortion at low and high frequencies is similar since the total energy released is similar in all cases. The shape of the spectrum for different values of spectral index is also similar in the Rayleigh-Jeans and Wien tails, as expected for the intermediate type spectra, Fig. 7. But the spectra are very different and easily distinguishable near the zero crossing, which is at $x_0 = 3.04, \nu = 173 \text{ GHz}$ for $n_{ss} = 1$. For $n_{ss} > 1$ there is more power on smaller scales which dissipate earlier moving the x_0 towards lower values (or towards μ -type value of $x_0 = 2.19, \nu = 124 \text{ GHz}$) and for $n_{ss} = 1.5$, $x_0 = 2.74, \nu = 156 \text{ GHz}$. On the other side, for $n_{ss} < 1$, the spectrum moves towards the y -type value of $x_0 = 3.83, \nu = 217 \text{ GHz}$, and for $n_{ss} = 0.5$ the zero crossing is at $x_0 = 3.32, \nu = 189 \text{ GHz}$. There is of course more information in the full spectrum than just the zero crossing and a sensitive experiment should be able to use the full spectrum to tightly constrain more complicated shapes of the small scale primordial spectrum than the simple two parameter (amplitude and spectral index) model considered here. The zero crossing, and frequencies of minimum and maximum flux difference with respect to the reference blackbody can be fitted by the following simple formula as a function of n_{ss} for $0.5 \lesssim n_{ss} \lesssim 1.5$ at better than 1% accuracy,

$$x_{0/\text{min/max}}(n_{ss}) = a_0 + a_1 n_{ss}, \quad (6.5)$$

where $a_0 = 3.61, a_1 = -0.588$ for x_0 , $a_0 = 2.11, a_1 = -0.466$ for x_{min} and $a_0 = 6.24, a_1 = -0.63$ for x_{max}

7 Application: annihilation and decay of particles

There are many sources of heating possible in the early Universe from particle physics beyond the standard model, as discussed in the introduction. Different sources of energy injection may have

³Analytic solution including comptonization and both bremsstrahlung and double Compton processes with percent level accuracy is given in [7].

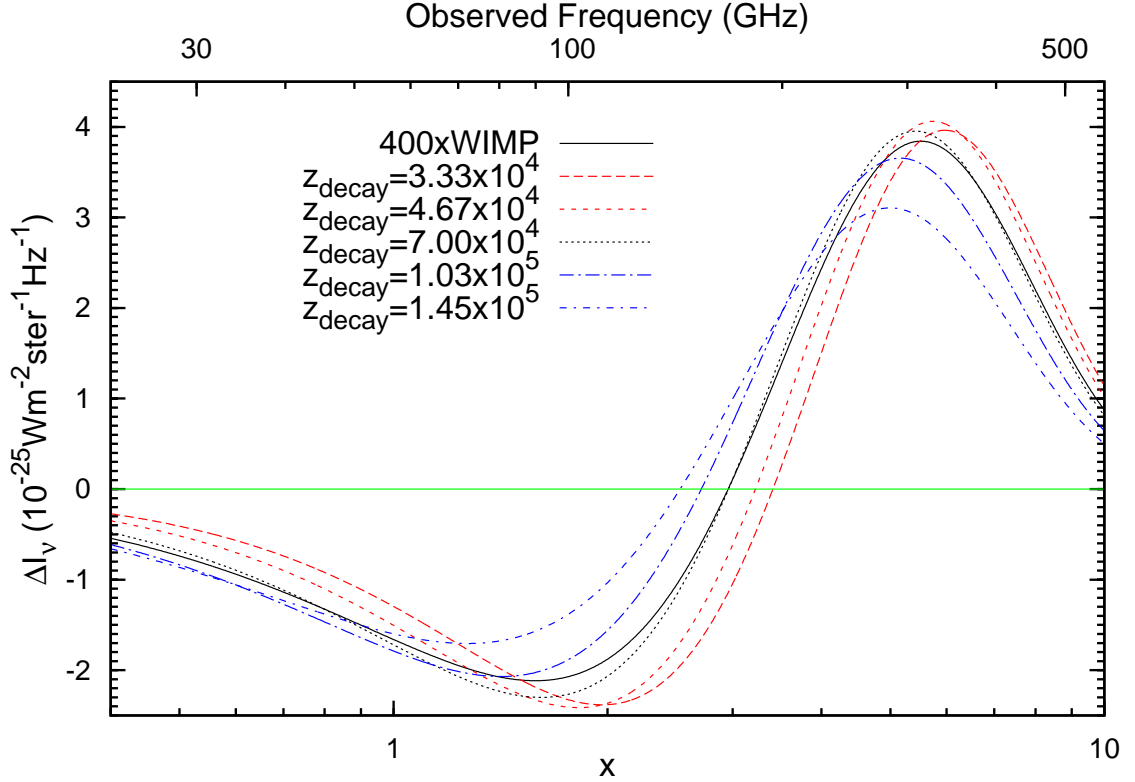


Figure 13. Distortion spectrum created by annihilation of WIMP dark matter (multiplied by 400 to bring its amplitude to $\sim 10^{-7}$) and decay of unstable particles with different decay times $(z_X, \tau_X) = (3.33 \times 10^4, 661 \text{ years}), (4.67 \times 10^4, 339 \text{ years}), (7.00 \times 10^4, 152 \text{ years}), (1.03 \times 10^5, 70.5 \text{ years}), (1.45 \times 10^5, 35.7 \text{ years})$; the curves are labeled by z_X . The shape of the WIMP annihilation spectral distortion is close to the $n_{ss} = 1$ spectrum in Fig. 12. Difference in intensity from the reference blackbody with same number density of photons is plotted.

different dependence on redshift and will give rise to different shapes of intermediate-type spectrum. We thus have a way of distinguishing between different types of energy injection mechanisms. We will illustrate this by considering annihilation of weakly interacting massive particles (WIMP dark matter), which has a power law dependence on redshift/time, and decay of unstable particles having an exponential dependence on time.

For the thermally produced WIMP dark matter consisting of self-annihilating Majorana particles,⁴ the energy release due to annihilation is given by,

$$\begin{aligned} \frac{d\mathcal{E}}{dz} &= -f_\gamma \frac{m_{\text{dm}} c^2 n_{\text{dm}}^2 \langle \sigma v \rangle}{\rho_\gamma (1+z) H} \\ &\approx -f_\gamma \frac{6.9 \times 10^{-10} (1+z)^{-1}}{\sqrt{1 + (1+z_{\text{eq}})/(1+z)}} \left(\frac{10 \text{ GeV}}{m_{\text{dm}}} \right), \end{aligned} \quad (7.1)$$

where we have assumed velocity averaged cross section $\langle \sigma v \rangle \approx 3 \times 10^{-27} / (\Omega_{\text{dm}} h_0^2) \text{ cm}^{-3} \text{ s}^{-1}$ [78], Ω_{dm} is the dark matter density as a function of critical density today, H is the Hubble parameter, $h_0 = H_0/100 = 0.702$, f_γ is the fraction of energy going into heating the plasma, m_{dm} is the mass of

⁴For Dirac particles the energy release is smaller by a factor of 2.

dark matter particle, n_{dm} is the dark matter number density and $z_{\text{eq}} \approx 3234$ is the redshift of matter radiation equality. At $z \gg z_{\text{eq}}$ we have $d\mathcal{E}/dz \propto 1 + z$. For the dissipation of sound waves in Eq. (6.1) under same approximation we have $d\mathcal{E}/dz \propto (1+z)^{(3n_{\text{ss}}-5)/2}$. For $n_{\text{ss}} = 1$ dark matter annihilation and sound wave dissipation have the same redshift dependence and we expect the shape of intermediate-type spectrum for these two cases. More precisely, for dark matter annihilation, approximately 30% of the energy released at $z \gtrsim 500$ appears as μ -type distortion, 37% as intermediate-type distortion and the rest of the energy goes to the y_γ -type distortion.

For decay of a particle of mass m_X , initial comoving number density n_{X0} , and life time τ_X with f_γ fraction of energy going into heating of the plasma, we have

$$\frac{d\mathcal{E}}{dz} = -f_\gamma \frac{n_{X0} m_X c^2 e^{-t/\tau_X}}{a_R T_{\text{CMB}}^4 H(1+z)^2 \tau_X} \quad (7.2)$$

To get total distortion of $\sim 10^{-7}$, we choose $f_\gamma n_{X0} m_X c^2 = 10^{-7} a_R T_{\text{CMB}}^4 (1+z_X)$, where z_X is the decay redshift corresponding to the lifetime τ_X , and during radiation domination we have $\tau_X \approx 1/(2(1+z_X)^2 H_0 \Omega_r^{1/2})$. The division of released energy into y , μ and intermediate-type distortions varies quite dramatically with the lifetime of the particle and illustrates nicely how using the intermediate-distortions along with μ and y -type distortions can help remove degeneracies associated with different energy release mechanisms. For $z_X = 1.45 \times 10^5$, 21% of released energy appears as μ -type distortion and 79% as intermediate type distortions. For $z_X = 4.67 \times 10^4$, 7×10^4 , almost all of the energy, $\sim 99\%$, 97% respectively, goes to intermediate-type distortions with the most of the rest in μ -type distortions. For $z_X = 1.5 \times 10^4$ the division is 42 : 58 between intermediate and y -type distortions respectively and μ -type distortions get a negligible share.

The intermediate-type spectral distortion for WIMP annihilation and decay of an unstable particles with different lifetimes z_X is shown in Fig. 13 (intensity). The WIMP spectral distortion is multiplied by 400 to bring it to the same level as the decaying particle signal. WIMP annihilation spectrum is similar to $n_{\text{ss}} = 1$ spectrum in Fig. 12 as expected from their similar redshift dependence. Also, the WIMP annihilation (power law dependence of energy injection on redshift) and the spectra for decaying particles (exponential dependence on redshift) with different lifetimes are distinguishable from each other. There is a small degeneracy for $z_X \approx 7 \times 10^4$; the exponential decay in this case has same zero crossing as annihilation, and the shapes of two curves are very close. The μ -type distortions in the two cases are very different, as discussed above, and break this degeneracy. Nevertheless, the intermediate-type spectrum has the possibility of *measuring* the life-time of the decaying particle in addition to the total energy injected into the CMB. The frequencies $x_0, x_{\text{min}}, x_{\text{max}}$ can be fitted by the formula for dark matter decay at with $z_4 \equiv z_X/10^4$ for $10^4 \lesssim z_X \lesssim 2 \times 10^5$ with better than 1% precision,

$$x_{0\text{min/man}} = a_0 + a_1 \ln(z_4) + a_2 \ln^2(z_4) + a_3 \ln^3(z_4) + a_4 \ln^4(z_4), \quad (7.3)$$

where for x_0 the fit coefficients are $a_0 = 3.67, a_1 = -0.0644, a_2 = -0.017, a_3 = -0.1365, a_4 = 0.0343$, for x_{min} they are $a_0 = 2.16, a_1 = -0.07, a_2 = 0.0146, a_3 = -0.1165, a_4 = 0.0276$, and for x_{max} we have $a_0 = 6.25, a_1 = 0.0158, a_2 = -0.157, a_3 = -0.1, a_4 = 0.0335$. For dark matter annihilation, the frequencies are $x_0 = 2.96, x_{\text{min}} = 1.58, x_{\text{max}} = 5.52$.

8 Non-degeneracy among Intermediate-type distortions and a mixture of y and μ -type distortions

Since the intermediate type distortions lie in-between y and μ type distortions, an important question arises: can an intermediate-type contribution to the CMB spectral distortion be mistaken for a combination of y and μ type distortions and vice versa? The answer is no, these three types of distortions

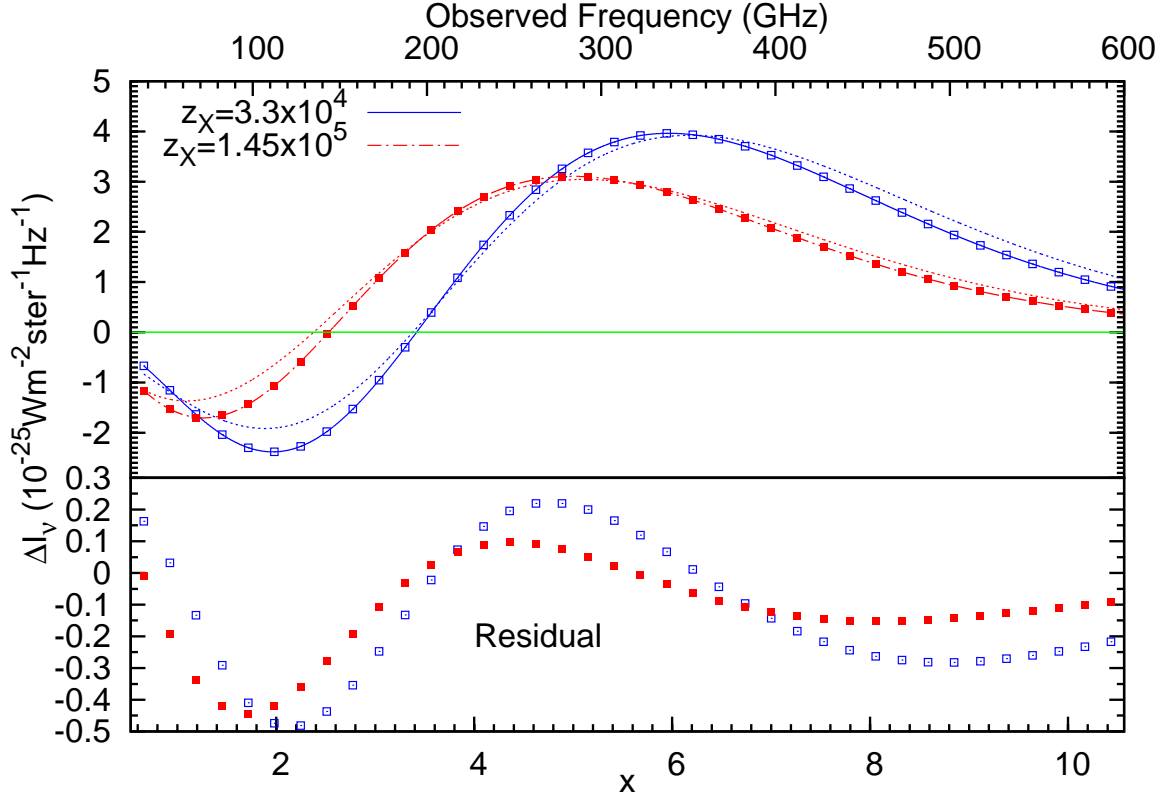


Figure 14. Intermediate-type distortions from particle decay are shown for two different decay times, as in Fig. 13. Also shown is the least squares fit of the mixtures of y and μ type distortions (dotted curves) which approximate these intermediate-type distortions at PIXIE frequencies.

are non-degenerate with each other and can be distinguished. This is clear by looking at Fig. 7. The intermediate distortions ($\Delta T/T$) for $0.01 \leq y_\gamma \leq 2$ are almost constant at both low and high frequencies. The y -type distortions, on the other hand, rise at high frequencies as $\Delta T/T \propto x$. The magnitude of the μ -type distortions similarly increases at low frequencies with $\Delta T/T \propto 1/x$. Any mixture of pure y and μ type distortions will thus have much greater slopes than the intermediate type distortions, and in principle they can be separated from each other.

We show in Fig. 14 the same spectrum as in Fig. 13, for the energy injection due to particle decay for two different decay times, $z_X = 1.45 \times 10^5, 3.33 \times 10^4$. Also shown is a combination of μ and y -type distortions, which approximate these intermediate-type spectral distortions in the least squares sense. Thus, a sensitive experiment should be able to distinguish between μ , y and intermediate-type distortions when the distortions are detected at high significance. In particular, it should be possible to not only avoid the contamination of the μ type distortions from the intermediate-type distortions but also measure the intermediate-type distortions themselves.

The issue of degeneracy and the sensitivity required to detect intermediate type distortions can be made more precise by asking a slightly different question: How closely can a total spectrum containing all μ , y and intermediate-type distortions can be fitted by just μ and y -type distortions. We show in Fig. 15 the total spectrum from Silk damping with $n_{ss} = 1$, and amplitude $10A_\zeta = 1.61 \times 10^{-8}$. The total spectrum has a Bose-Einstein part with $\mu = 10^{-7}$ and y -type part with $y = 3 \times 10^{-8}$. In reality, the y -type part of the spectrum would be much higher because of the contributions from reionization and later times, but this does not change our arguments or conclusions. Also shown is

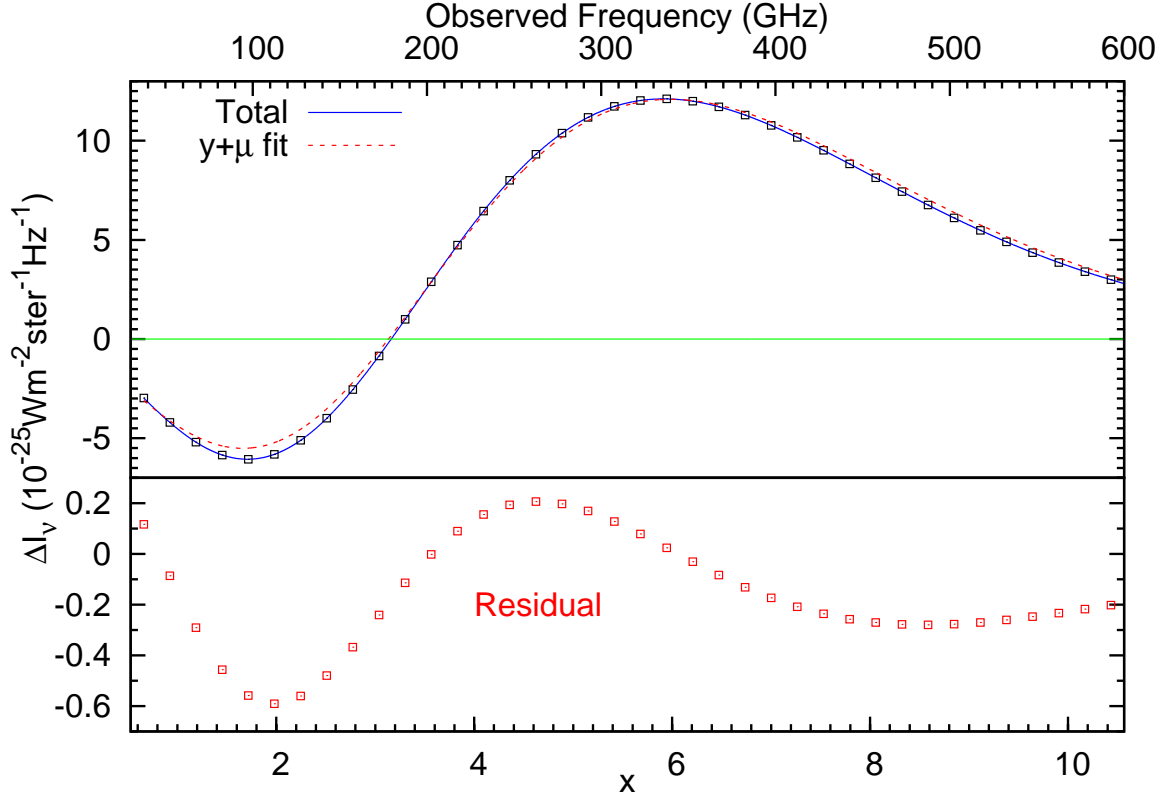


Figure 15. Total spectrum containing an intermediate-type distortion from Silk damping with $n_{\text{ss}} = 1$, and amplitude $10A_{\zeta} = 1.61 \times 10^{-8}$, and μ and y -type distortions with $\mu = 10^{-7}$ and $y = 3 \times 10^{-8}$. All three components have approximately the similar amount of energy. Also shown is the best fit $y_{\gamma} + \mu$ spectrum to the data points at PIXIE frequencies. The best fit spectrum has $\mu = 1.8 \times 10^{-7}$ and $y = 4.26 \times 10^{-8}$. The residual (data-fit) is shown in the bottom panel.

the least squares fit using the data points at PIXIE frequencies (also shown) to the spectrum with only y and μ -type distortions. The best fit spectrum has $y = 4.26 \times 10^{-8}$ and $\mu = 1.8 \times 10^{-7}$. The bottom panel shows the difference between the data points and $y + \mu$ fit. It is clear from these plots that the full spectrum cannot be fit exactly with only y and μ -type components and the residuals (data-fit) contain give information about the type of intermediate-distortion present. In particular the residuals, which are $\sim 20\%$ of the intermediate-type distortion, are not affected by the presence of additional y and μ components in the spectrum. Thus the detection of the intermediate-type spectrum will be challenging but possible. In addition, since we do not know the temperature of the blackbody part of the spectrum at the required precision a priori, we should fit for the temperature of blackbody along with the distortions [1].

9 Observational issues

Our definition of spectral distortions and x_0 is convenient to compare and understand the process of comptonization and theoretical spectra of different types. Observationally, it is not possible to calculate the reference blackbody temperature required for these definitions to desired accuracy. Achieving an accuracy of $\sim 10^{-8}$ in the number density of photons, and hence the reference temperature, requires integrating the spectrum between $10^{-4} \lesssim x \lesssim 25$! This means that $x_0, x_{\text{min}}, x_{\text{max}}$ as defined

by us is not a direct observable for small distortions. x_0, x_{\min}, x_{\max} can however be inferred once the full spectrum is measured with sufficient precision and the intermediate-type spectral distortion part separated.

The shape of the intermediate-type spectral distortions contains much more, and complementary, information compared to the μ/y -type distortion. High precision experiments in the future may thus be able to not only put stringent constraints on the energy release in the early Universe using μ distortions, but also distinguish between different mechanisms of energy injection using the intermediate-type spectral distortions. Detecting the μ, y and intermediate-type distortions at the level of $10^{-7} - 10^{-9}$ would require understanding and subtracting foregrounds at high precision. Simulations for the proposed experiment PIXIE [5] show that such a subtraction may be possible at nK level. However, there are still some uncertainties in our understanding of the foregrounds as demonstrated by the unexplained excess flux at low frequencies in the ARCADE experiment measurements [79] and more work needs to be done to demonstrate the feasibility of the measurements proposed in the present paper.

10 Conclusions

The CMB blackbody spectrum in the Λ CDM cosmology is established at $z > 2 \times 10^6$, when the photon number changing processes of bremsstrahlung and double Compton scattering are effective. Compton scattering establishes a Bose-Einstein spectrum corresponding to the energy and number density of photons available while bremsstrahlung and double Compton scattering help drive the chemical potential to zero. If there is energy/photon production due to non-standard physics at $z < 2 \times 10^6$, the blackbody spectrum cannot be restored and an imprint is left on the CMB spectrum. Initially a y -type distortion is established which evolves (comptonizes) towards a Bose-Einstein spectrum. How close the initial y -type distortion can get to a Bose-Einstein spectrum depends on the redshift of energy release. At $z \gtrsim 2 \times 10^5$, full comptonization is possible but at lower redshifts Compton scattering can no longer establish a Bose-Einstein spectrum. At redshifts $1.5 \times 10^4 \lesssim z \lesssim 2 \times 10^5$, there is partial comptonization and we get a spectrum which is in-between a y -type spectrum and a Bose-Einstein spectrum. The detailed shape of this intermediate-type spectrum depends on how the rate of energy injection varies with the redshift. The detection of a deviation of the CMB spectrum from a blackbody thus contains information about the amount as well as the redshift/mechanism of the energy release.

We have numerically calculated the detailed evolution of the initial y -type distortion by solving the Kompaneets equation taking into account the correct evolution of the electron temperature, which decreases from the initial y -type distortion value towards a Bose-Einstein value. An analytic solution valid in the weak comptonization limit, $y_\gamma \lesssim 0.1$, is given in Eq. (5.3). We have demonstrated that the intermediate-type spectral distortions, resulting from sound wave dissipation in the early Universe can, in principle, constrain the shape of the small scale power spectrum. It is also possible to distinguish between different energy injection mechanisms, which have different dependence on redshift, for example, WIMP annihilation and Silk damping with different power law dependence and particle decay with exponential dependence. The y, μ and intermediate-type distortions have important differences in their shapes and it is in principle possible to distinguish between them. In particular, a mixture of y and μ -type distortions fails to mimic the intermediate-type distortions by 20%, and vice versa. Proposed experiment PIXIE [5] will detect y and μ -type distortions at the level of $y = 10^{-8}, \mu = 5 \times 10^{-8}$ improving the current limits by 3 orders of magnitude. The additional y -distortions from low redshifts should not affect an experiment's ability to detect μ and intermediate-type distortions. Measurement of intermediate-type distortions will thus be challenging but possible.

We make publicly available⁵ high precision intermediate-type distortion templates and a Mathematica code which superposes these templates, according to user-defined redshift-dependent energy injection rate, to calculate the μ , y and intermediate-type distortions.

Acknowledgments

We would like to thank Jens Chluba for comments on the manuscript.

References

- [1] D. J. Fixsen, E. S. Cheng, J. M. Gales, J. C. Mather, R. A. Shafer, and E. L. Wright, *The Cosmic Microwave Background Spectrum from the Full COBE FIRAS Data Set*, *ApJ* **473** (1996) 576.
- [2] R. A. Sunyaev and Y. B. Zeldovich, *The interaction of matter and radiation in the hot model of the Universe, II*, *ApSS* **7** (1970) 20.
- [3] Y. B. Zeldovich and R. A. Sunyaev, *The Interaction of Matter and Radiation in a Hot-Model Universe*, *ApSS* **4** (1969) 301.
- [4] D. J. Fixsen and J. C. Mather, *The Spectral Results of the Far-Infrared Absolute Spectrophotometer Instrument on COBE*, *ApJ* **581** (2002) 817.
- [5] A. Kogut, D. J. Fixsen, D. T. Chuss, J. Dotson, E. Dwek, M. Halpern, G. F. Hinshaw, S. M. Meyer, S. H. Moseley, M. D. Seiffert, D. N. Spergel, and E. J. Wollack, *The Primordial Inflation Explorer (PIXIE): a nulling polarimeter for cosmic microwave background observations*, *JCAP* **7** (2011) 25, [[arXiv:1105.2044](https://arxiv.org/abs/1105.2044)].
- [6] L. Danese and G. de Zotti, *Double Compton process and the spectrum of the microwave background*, *A&A* **107** (1982) 39.
- [7] R. Khatri and R. A. Sunyaev, *Creation of the CMB spectrum: precise analytic solutions for the blackbody photosphere*, *JCAP* **6** (2012) 38, [[arXiv:1203.2601](https://arxiv.org/abs/1203.2601)].
- [8] J. Silk, *Cosmic Black-Body Radiation and Galaxy Formation*, *ApJ* **151** (1968) 459.
- [9] R. A. Sunyaev and Y. B. Zeldovich, *Small scale entropy and adiabatic density perturbations Antimatter in the Universe*, *Ap&SS* **9** (1970) 368.
- [10] R. A. Daly, *Spectral distortions of the microwave background radiation resulting from the damping of pressure waves*, *ApJ* **371** (1991) 14.
- [11] W. Hu, D. Scott, and J. Silk, *Power spectrum constraints from spectral distortions in the cosmic microwave background*, *ApJL* **430** (1994) L5–L8, [[astro-ph/9402045](https://arxiv.org/abs/astro-ph/9402045)].
- [12] J. Chluba and R. A. Sunyaev, *The evolution of CMB spectral distortions in the early Universe*, *MNRAS* **419** (2012) 1294, [[arXiv:1109.6552](https://arxiv.org/abs/1109.6552)].
- [13] J. Chluba, R. Khatri, and R. A. Sunyaev, *CMB at 2x2 order: The dissipation of primordial acoustic waves and the observable part of the associated energy release*, *arXiv:1202.0057* (2012) [[arXiv:1202.0057](https://arxiv.org/abs/1202.0057)].
- [14] E. Pajer and M. Zaldarriaga, *A Hydrodynamical Approach to CMB μ -distortions*, *ArXiv e-prints* (2012) [[arXiv:1206.4479](https://arxiv.org/abs/1206.4479)].
- [15] R. Khatri, R. A. Sunyaev, and J. Chluba, *Does Bose-Einstein condensation of CMB photons cancel μ distortions created by dissipation of sound waves in the early Universe?*, *A&A* **540** (2012) A124, [[arXiv:1110.0475](https://arxiv.org/abs/1110.0475)].

⁵<http://www.mpa-garching.mpg.de/~khatri/idistort.html>

- [16] A. F. Illarionov and R. A. Sunyaev, *Comptonization, the background-radiation spectrum, and the thermal history of the universe*, *Soviet Astronomy* **18** (1975) 691.
- [17] C. Burigana, L. Danese, and G. de Zotti, *Formation and evolution of early distortions of the microwave background spectrum - A numerical study*, *A&A* **246** (1991) 49.
- [18] W. Hu and J. Silk, *Thermalization and spectral distortions of the cosmic background radiation*, *Phys.Rev.D* **48** (1993) 485.
- [19] P. Procopio and C. Burigana, *A numerical code for the solution of the Kompaneets equation in cosmological context*, *A&A* **507** (2009) 1243, [[arXiv:0905.2886](#)].
- [20] A. S. Kompaneets, *The establishment of thermal equilibrium between quanta and electrons*, *Zh. Eksp. Teor. Fiz.* **31** (1956) 876.
- [21] E. L. Wright, *Distortion of the microwave background by a hot intergalactic medium*, *ApJ* **232** (1979) 348.
- [22] Y. Rephaeli, *Cosmic microwave background comptonization by hot intracluster gas*, *ApJ* **445** (1995) 33.
- [23] A. Challinor and A. Lasenby, *Relativistic Corrections to the Sunyaev-Zeldovich Effect*, *ApJ* **499** (1998) 1, [[astro-ph/9711161](#)].
- [24] N. Itoh, Y. Kohyama, and S. Nozawa, *Relativistic Corrections to the Sunyaev-Zeldovich Effect for Clusters of Galaxies*, *ApJ* **502** (1998) 7, [[astro-ph/9712289](#)].
- [25] S. Y. Sazonov and R. A. Sunyaev, *Cosmic Microwave Background Radiation in the Direction of a Moving Cluster of Galaxies with Hot Gas: Relativistic Corrections*, *ApJ* **508** (1998) 1.
- [26] S. Nozawa, N. Itoh, and Y. Kohyama, *Relativistic Corrections to the Sunyaev-Zeldovich Effect for Clusters of Galaxies. II. Inclusion of Peculiar Velocities*, *ApJ* **508** (1998) 17, [[astro-ph/9804051](#)].
- [27] S. M. Molnar and M. Birkinshaw, *Inverse Compton Scattering in Mildly Relativistic Plasma*, *ApJ* **523** (1999) 78, [[astro-ph/9903444](#)].
- [28] T. A. Enßlin and C. R. Kaiser, *Comptonization of the cosmic microwave background by relativistic plasma*, *A&A* **360** (2000) 417, [[astro-ph/0001429](#)].
- [29] A. D. Dolgov, S. H. Hansen, S. Pastor, and D. V. Semikoz, *Spectral Distortion of Cosmic Microwave Background Radiation by Scattering on Hot Electrons: Exact Calculations*, *ApJ* **554** (2001) 74, [[astro-ph/0010412](#)].
- [30] M. Shimon and Y. Rephaeli, *Quantitative description of the Sunyaev-Zeldovich effect: analytic approximations*, *New Astronomy* **9** (2004) 69, [[astro-ph/0309098](#)].
- [31] J. Chluba, G. Hütsi, and R. A. Sunyaev, *Clusters of galaxies in the microwave band: Influence of the motion of the Solar System*, *A&A* **434** (2005) 811, [[astro-ph/0409058](#)].
- [32] J. Chluba, D. Nagai, S. Sazonov, and K. Nelson, *A fast and accurate method for computing the Sunyaev-Zeldovich signal of hot galaxy clusters*, *arXiv:1205.5778* (2012).
- [33] E. Komatsu, K. M. Smith, J. Dunkley, C. L. Bennett, B. Gold, G. Hinshaw, N. Jarosik, D. Larson, M. R. Nolta, L. Page, D. N. Spergel, M. Halpern, R. S. Hill, A. Kogut, M. Limon, S. S. Meyer, N. Odegard, G. S. Tucker, J. L. Weiland, E. Wollack, and E. L. Wright, *Seven-year Wilkinson Microwave Anisotropy Probe (WMAP) Observations: Cosmological Interpretation*, *ApJS* **192** (2011) 18.
- [34] G. Mangano, G. Miele, S. Pastor, T. Pinto, O. Pisanti, and P. D. Serpico, *Relic neutrino decoupling including flavour oscillations*, *Nuclear Physics B* **729** (2005) 221, [[hep-ph/0506164](#)].
- [35] J. L. Feng, *Dark Matter Candidates from Particle Physics and Methods of Detection*, *ARA&A* **48** (2010) 495, [[arXiv:1003.0904](#)].
- [36] J. L. Feng, A. Rajaraman, and F. Takayama, *Superweakly interacting massive particle dark matter signals from the early universe*, *Phys. Rev. D* **68** (2003), no. 6 063504.

- [37] B. J. Carr, K. Kohri, Y. Sendouda, and J. Yokoyama, *New cosmological constraints on primordial black holes*, *Phys. Rev. D* **81** (2010), no. 10 104019.
- [38] A. Vilenkin and E. P. S. Shellard, *Cosmic Strings and Other Topological Defects*. Cambridge University Press, Cambridge, 2000.
- [39] A. Vilenkin, *Gamma-rays from superconducting cosmic strings*, *Nature* **332** (1988) 610.
- [40] H. Tashiro, E. Sabancilar, and T. Vachaspati, *CMB Distortions from Superconducting Cosmic Strings*, *arXiv:1202.2474* (2012).
- [41] K. Jedamzik, V. Katalinić, and A. V. Olinto, *Limit on Primordial Small-Scale Magnetic Fields from Cosmic Microwave Background Distortions*, *Physical Review Letters* **85** (2000) 700, [[astro-ph/9911100](#)].
- [42] T. R. Slatyer, N. Padmanabhan, and D. P. Finkbeiner, *CMB constraints on WIMP annihilation: Energy absorption during the recombination epoch*, *Phys.Rev.D* **80** (2009), no. 4 043526, [[arXiv:0906.1197](#)].
- [43] R. Khatri, R. A. Sunyaev, and J. Chluba, *Mixing of blackbodies: entropy production and dissipation of sound waves in the early Universe*, *A&A* **543** (2012) A136, [[arXiv:1205.2871](#)].
- [44] A. F. Illarionov and R. A. Sunyaev, *Comptonization, characteristic radiation spectra, and thermal balance of low-density plasma*, *Soviet Astronomy* **18** (1975) 413.
- [45] Y. B. Zeldovich, V. G. Kurt, and R. A. Sunyaev, *Recombination of Hydrogen in the Hot Model of the Universe*, *Zh. Eksp. Teor. Fiz.* **55** (1968) 278.
- [46] P. J. E. Peebles, *Recombination of the Primeval Plasma*, *ApJ* **153** (1968) 1.
- [47] S. Seager, D. D. Sasselov, and D. Scott, *How Exactly Did the Universe Become Neutral?*, *ApJS* **128** (2000) 407, [[astro-ph/9912182](#)].
- [48] Y. Ali-Haïmoud and C. M. Hirata, *Ultrafast effective multilevel atom method for primordial hydrogen recombination*, *Phys.Rev.D* **82** (2010), no. 6 063521, [[arXiv:1006.1355](#)].
- [49] Y. Ali-Haïmoud and C. M. Hirata, *HyRec: A fast and highly accurate primordial hydrogen and helium recombination code*, *Phys.Rev.D* **83** (2011), no. 4 043513, [[arXiv:1011.3758](#)].
- [50] J. Chluba and R. M. Thomas, *Towards a complete treatment of the cosmological recombination problem*, *MNRAS* **412** (2011) 748, [[arXiv:1010.3631](#)].
- [51] R. Cen and J. P. Ostriker, *Where Are the Baryons?*, *ApJ* **514** (1999) 1, [[astro-ph/9806281](#)].
- [52] R. Cen and J. P. Ostriker, *Where Are the Baryons? II. Feedback Effects*, *ApJ* **650** (2006) 560, [[astro-ph/0601008](#)].
- [53] B. B. Nath and J. Silk, *Heating of the intergalactic medium as a result of structure formation*, *MNRAS* **327** (2001) L5–L9, [[astro-ph/0107394](#)].
- [54] E. Komatsu and U. Seljak, *The Sunyaev-Zeldovich angular power spectrum as a probe of cosmological parameters*, *MNRAS* **336** (2002) 1256, [[astro-ph/0205468](#)].
- [55] E. J. Hallman, B. W. O’Shea, B. D. Smith, J. O. Burns, and M. L. Norman, *The Santa Fe Light Cone Simulation Project. II. The Prospects for Direct Detection of the Whim with SZE Surveys*, *ApJ* **698** (2009) 1795, [[arXiv:0903.3239](#)].
- [56] N. Sehgal, P. Bode, S. Das, C. Hernandez-Monteagudo, K. Huffenberger, Y.-T. Lin, J. P. Ostriker, and H. Trac, *Simulations of the Microwave Sky*, *ApJ* **709** (2010) 920, [[arXiv:0908.0540](#)].
- [57] The CORe Collaboration, C. Armitage-Caplan, M. Avillez, D. Barbosa, A. Banday, N. Bartolo, R. Battye, J. Bernard, P. de Bernardis, S. Basak, M. Bersanelli, P. Bielewicz, A. Bonaldi, M. Bucher, F. Bouchet, F. Boulanger, C. Burigana, P. Camus, A. Challinor, S. Chongchitnan, D. Clements, S. Colafrancesco, J. Delabrouille, M. De Petris, G. De Zotti, C. Dickinson, J. Dunkley, T. Ensslin, J. Fergusson, P. Ferreira, K. Ferriere, F. Finelli, S. Galli, J. Garcia-Bellido, C. Gauthier, M. Haverkorn, M. Hindmarsh, A. Jaffe, M. Kunz, J. Lesgourgues, A. Liddle, M. Liguori, M. Lopez-Caniego,

- B. Maffei, P. Marchegiani, E. Martinez-Gonzalez, S. Masi, P. Mausekopf, S. Matarrese, A. Melchiorri, P. Mukherjee, F. Nati, P. Natoli, M. Negrello, L. Pagano, D. Paoletti, T. Peacocke, H. Peiris, L. Perrotto, F. Piacentini, M. Piat, L. Piccirillo, G. Pisano, N. Ponthieu, C. Rath, S. Ricciardi, J. Rubino Martin, M. Salatino, P. Shellard, R. Stompor, L. T. J. Urrestilla, B. Van Tent, L. Verde, B. Wandelt, and S. Withington, *CORÉ (Cosmic Origins Explorer) A White Paper*, *ArXiv e-prints* (2011) [[arXiv:1102.2181](#)].
- [58] Planck Science Team, *Planck blue book*, 2005.
- [59] M. D. Niemack, P. A. R. Ade, J. Aguirre, F. Barrientos, J. A. Beall, J. R. Bond, J. Britton, H. M. Cho, S. Das, M. J. Devlin, S. Dicker, J. Dunkley, R. Dünner, J. W. Fowler, A. Hajian, M. Halpern, M. Hasselfield, G. C. Hilton, M. Hilton, J. Hubmayr, J. P. Hughes, L. Infante, K. D. Irwin, N. Jarosik, J. Klein, A. Kosowsky, T. A. Marriage, J. McMahon, F. Menanteau, K. Moodley, J. P. Nibarger, M. R. Nolte, L. A. Page, B. Partridge, E. D. Reese, J. Sievers, D. N. Spergel, S. T. Staggs, R. Thornton, C. Tucker, E. Wollack, and K. W. Yoon, *ACTPol: a polarization-sensitive receiver for the Atacama Cosmology Telescope*, in *Society of Photo-Optical Instrumentation Engineers (SPIE) Conference Series*, vol. 7741 of *Society of Photo-Optical Instrumentation Engineers (SPIE) Conference Series*, 2010. [arXiv:1006.5049](#).
- [60] J. J. McMahon, K. A. Aird, B. A. Benson, L. E. Bleem, J. Britton, J. E. Carlstrom, C. L. Chang, H. S. Cho, T. de Haan, T. M. Crawford, A. T. Crites, A. Datesman, M. A. Dobbs, W. Everett, N. W. Halverson, G. P. Holder, W. L. Holzapfel, D. Hrubes, K. D. Irwin, M. Joy, R. Keisler, T. M. Lanting, A. T. Lee, E. M. Leitch, A. Loehr, M. Lueker, J. Mehl, S. S. Meyer, J. J. Mohr, T. E. Montroy, M. D. Niemack, C. C. Ngeow, V. Novosad, S. Padin, T. Plagge, C. Pryke, C. Reichardt, J. E. Ruhl, K. K. Schaffer, L. Shaw, E. Shirokoff, H. G. Spieler, B. Stadler, A. A. Stark, Z. Staniszewski, K. Vanderlinde, J. D. Vieira, G. Wang, R. Williamson, V. Yefremenko, K. W. Yoon, O. Zhan, and A. Zenteno, *SPTpol: an instrument for CMB polarization*, in *American Institute of Physics Conference Series* (B. Young, B. Cabrera, and A. Miller, eds.), vol. 1185 of *American Institute of Physics Conference Series*, p. 511, 2009.
- [61] W. Hu, D. Scott, and J. Silk, *Reionization and cosmic microwave background distortions: A complete treatment of second-order Compton scattering*, *Phys.Rev.D* **49** (1994) 648, [[astro-ph/9305038](#)].
- [62] J. Chluba and R. A. Sunyaev, *Superposition of blackbodies and the dipole anisotropy: A possibility to calibrate CMB experiments*, *A&A* **424** (2004) 389, [[astro-ph/0404067](#)].
- [63] R. Weymann, *Diffusion Approximation for a Photon Gas Interacting with a Plasma via the Compton Effect*, *Physics of Fluids* **8** (1965) 2112.
- [64] R. Khatri and R. A. Sunyaev, *Time of primordial ${}^7\text{Be}$ conversion into ${}^7\text{Li}$, energy release and doublet of narrow cosmological neutrino lines*, *Astronomy Letters* **37** (2011) 367, [[arXiv:1009.3932](#)].
- [65] Y. B. Zeldovich and E. V. Levich, *Stationary state of electrons in a non-equilibrium radiation field.*, *Soviet Journal of Experimental and Theoretical Physics Letters* **11** (1970) 35.
- [66] E. V. Levich and R. A. Sunyaev, *Heating of Gas near Quasars, Seyfert-Galaxy Nuclei, and Pulsars by Low-Frequency Radiation.*, *Soviet Astronomy* **15** (1971) 363.
- [67] R. Keisler, C. L. Reichardt, K. A. Aird, B. A. Benson, L. E. Bleem, J. E. Carlstrom, C. L. Chang, H. M. Cho, T. M. Crawford, A. T. Crites, T. de Haan, M. A. Dobbs, J. Dudley, E. M. George, N. W. Halverson, G. P. Holder, W. L. Holzapfel, S. Hoover, Z. Hou, J. D. Hrubes, M. Joy, L. Knox, A. T. Lee, E. M. Leitch, M. Lueker, D. Luong-Van, J. J. McMahon, J. Mehl, S. S. Meyer, M. Millea, J. J. Mohr, T. E. Montroy, T. Natoli, S. Padin, T. Plagge, C. Pryke, J. E. Ruhl, K. K. Schaffer, L. Shaw, E. Shirokoff, H. G. Spieler, Z. Staniszewski, A. A. Stark, K. Story, A. van Engelen, K. Vanderlinde, J. D. Vieira, R. Williamson, and O. Zahn, *A Measurement of the Damping Tail of the Cosmic Microwave Background Power Spectrum with the South Pole Telescope*, *ApJ* **743** (2011) 28, [[arXiv:1105.3182](#)].
- [68] R. Hlozek, J. Dunkley, G. Addison, J. W. Appel, J. R. Bond, C. Sofia Carvalho, S. Das, M. J. Devlin, R. Dünner, T. Essinger-Hileman, J. W. Fowler, P. Gallardo, A. Hajian, M. Halpern, M. Hasselfield, M. Hilton, A. D. Hincks, J. P. Hughes, K. D. Irwin, J. Klein, A. Kosowsky, T. A. Marriage, D. Marsden,

- F. Menanteau, K. Moodley, M. D. Niemack, M. R. Nolta, L. A. Page, L. Parker, B. Partridge, F. Rojas, N. Sehgal, B. Sherwin, J. Sievers, D. N. Spergel, S. T. Staggs, D. S. Swetz, E. R. Switzer, R. Thornton, and E. Wollack, *The Atacama Cosmology Telescope: A Measurement of the Primordial Power Spectrum*, *ApJ* **749** (2012) 90, [[arXiv:1105.4887](https://arxiv.org/abs/1105.4887)].
- [69] P. McDonald, U. Seljak, S. Burles, D. J. Schlegel, D. H. Weinberg, R. Cen, D. Shih, J. Schaye, D. P. Schneider, N. A. Bahcall, J. W. Briggs, J. Brinkmann, R. J. Brunner, M. Fukugita, J. E. Gunn, Ž. Ivezić, S. Kent, R. H. Lupton, and D. E. Vanden Berk, *The Ly α Forest Power Spectrum from the Sloan Digital Sky Survey*, *ApJS* **163** (2006) 80, [[astro-ph/0405013](https://arxiv.org/abs/astro-ph/0405013)].
- [70] U. Seljak, A. Slosar, and P. McDonald, *Cosmological parameters from combining the Lyman- α forest with CMB, galaxy clustering and SN constraints*, *JCAP* **10** (2006) 14, [[astro-ph/0604335](https://arxiv.org/abs/astro-ph/0604335)].
- [71] P. J. E. Peebles and J. T. Yu, *Primeval Adiabatic Perturbation in an Expanding Universe*, *ApJ* **162** (1970) 815.
- [72] N. Kaiser, *Small-angle anisotropy of the microwave background radiation in the adiabatic theory*, *MNRAS* **202** (1983) 1169.
- [73] E. M. Lifshitz *J. Phys. (USSR)* **10** (1946) 116.
- [74] A. D. Sakharov, *The Initial Stage of an Expanding Universe and the Appearance of a Nonuniform Distribution of Matter*, *Soviet Journal of Experimental and Theoretical Physics* **22** (1966) 241.
- [75] R. A. Sunyaev and Y. B. Zeldovich, *Small-Scale Fluctuations of Relic Radiation*, *ApSS* **7** (1970) 3.
- [76] Y. B. Zeldovich, A. F. Illarionov, and R. A. Sunyaev, *The Effect of Energy Release on the Emission Spectrum in a Hot Universe*, *Soviet Journal of Experimental and Theoretical Physics* **35** (1972) 643.
- [77] S. Weinberg, *Cosmology*. Oxford University Press, Oxford, 2008.
- [78] G. Jungman, M. Kamionkowski, and K. Griest, *Supersymmetric dark matter*, *Physics Reports* **267** (1996) 195, [[hep-ph/9506380](https://arxiv.org/abs/hep-ph/9506380)].
- [79] D. J. Fixsen, A. Kogut, S. Levin, M. Limon, P. Lubin, P. Mirel, M. Seiffert, J. Singal, E. Wollack, T. Villela, and C. A. Wuensche, *ARCADE 2 Measurement of the Absolute Sky Brightness at 3-90 GHz*, *ApJ* **734** (2011) 5.
- [80] J. Arons, *Radiative Transfer of Isotropic X-Rays and Gamma Rays. I. General Theory and Solutions for a Uniform Medium*, *ApJ* **164** (1971) 437.
- [81] A. F. Illarionov and R. A. Sunyaev, *Compton Scattering by Thermal Electrons in X-Ray Sources.*, *Soviet Astronomy* **16** (1972) 45.

A Fitting formulae for x_0, x_{\min}, x_{\max} as a function of y_γ

$x_0(y_\gamma), x_{\min}(y_\gamma), x_{\max}(y_\gamma)$ for the intermediate type spectra in Fig. 7 are well fitted (for small distortions) with an accuracy better than 1% for $y_\gamma \lesssim 10$ by the following formulae:

$$x_{0/\min/\max} = a_0 + a_1 y_\gamma + a_2 y_\gamma^2 + a_3 y_\gamma^3 + a_4 y_\gamma^4 + b_1 \sinh^{-1}(b_2 y_\gamma) + c_1 \tanh(c_2 y_\gamma), \quad (\text{A.1})$$

where we have for x_0 ,

$$a_0 = 3.83, a_1 = 0.363, a_2 = -5.68 \times 10^{-2}, a_3 = 5.15 \times 10^{-3}, a_4 = -1.85 \times 10^{-4}, \\ b_1 = 0.496, b_2 = -30.8, c_1 = 0.294, c_2 = 20.6, \quad (\text{A.2})$$

for x_{\min}

$$\begin{aligned} a_0 &= 2.265, a_1 = 0.332, a_2 = -5.07 \times 10^{-2}, a_3 = 4.4 \times 10^{-3}, a_4 = -1.5 \times 10^{-4}, \\ b_1 &= 0.439, b_2 = -21, c_1 = 0.24, c_2 = 14.1, \end{aligned} \quad (\text{A.3})$$

and for x_{\max}

$$\begin{aligned} a_0 &= 6.51, a_1 = 0.543, a_2 = -0.11, a_3 = 1.1 \times 10^{-2}, a_4 = -4 \times 10^{-4}, \\ b_1 &= 0.5, b_2 = -89, c_1 = 0.56, c_2 = 51. \end{aligned} \quad (\text{A.4})$$

B Analytic approximate solutions of Kompaneets equation

We expand the photon occupation number ($n(x, y_\gamma)$) around the initial black body spectrum at temperature T , $n(x, 0) \equiv n_{\text{pl}}(x) \equiv 1/(e^{hv/k_B T} - 1) = 1/(e^x - 1)$.

$$n(x, y_\gamma) = n(x, 0) + y_\gamma \frac{\partial n}{\partial y_\gamma}(x, 0) + \frac{y_\gamma^2}{2} \frac{\partial^2 n}{\partial y_\gamma^2}(x, 0) + \mathcal{O}(y_\gamma^3), \quad (\text{B.1})$$

where $x = hv/k_B T$ and T is the initial blackbody temperature. Further we can evaluate the corrections using Kompaneets equation.

$$\begin{aligned} \frac{\partial n}{\partial y_\gamma}(x, 0) &= \frac{1}{x^2} \frac{\partial}{\partial x} \left[x^4 \left(\frac{\partial n(x, y_\gamma)}{\partial x} \left(\frac{T_e}{T} \right) + n(x, y_\gamma) + n(x, y_\gamma)^2 \right) \right]_{y_\gamma=0} \\ &= \frac{1}{x^2} \frac{\partial}{\partial x} \left[x^4 \left(\frac{\partial n(x, 0)}{\partial x} \left(\frac{T_e}{T} - 1 \right) \right) \right] \\ &= \Delta_{T_e} \frac{1}{x^2} \frac{\partial}{\partial x} \left[x^4 \left(\frac{\partial n(x, 0)}{\partial x} \right) \right] \\ &= \Delta_{T_e} \frac{x e^x}{(e^x - 1)^2} \left[x \left(\frac{e^x + 1}{e^x - 1} \right) - 4 \right] \\ &\equiv \Delta_{T_e} n_y(x), \end{aligned} \quad (\text{B.2})$$

where $n_y(x)$ is just the linear y -type solution found in [3]. The next term in the Taylor series is

$$\begin{aligned} \frac{\partial^2 n}{\partial y_\gamma^2}(x, 0) &= \frac{\partial}{\partial y_\gamma} \frac{1}{x^2} \frac{\partial}{\partial x} \left[x^4 \left(\frac{\partial n}{\partial x} (\Delta_{T_e} + 1) + n + n^2 \right) \right]_{y_\gamma=0} \\ &= \Delta_{T_e} \frac{1}{x^2} \frac{\partial}{\partial x} \left[x^4 \left(\frac{\partial n(x, 0)}{\partial x} \frac{1}{\Delta_{T_e}} \frac{\partial \Delta_{T_e}}{\partial y_\gamma}(0) \right. \right. \\ &\quad \left. \left. + \left(\Delta_{T_e} \frac{1}{x^2} \frac{\partial}{\partial x} x^4 \frac{\partial^2 n(x, 0)}{\partial x^2} \right) \right. \right. \\ &\quad \left. \left. + \frac{2}{x} (\Delta_{T_e} + 1) \frac{\partial}{\partial x} \left(x^2 \frac{\partial n(x, 0)}{\partial x} \right) - 2x^2 \left(\frac{\partial n(x, 0)}{\partial x} \right)^2 \right] \right] \\ &\equiv \Delta_{T_e} f_y(x) + \Delta_{T_e}^2 f_2(x) + \frac{\partial \Delta_{T_e}}{\partial y_\gamma}(0) n_y(x). \end{aligned} \quad (\text{B.3})$$

The functions $f_y(x)$ and $f_2(x)$ are given explicitly in the Appendix C. Substituting the first and second order terms from Eqs. (B.3) and (3.4) in Eq. (B.1), we have the solution for partial comptonization

of an initial blackbody spectrum interacting with electrons at temperature $T_e(y_\gamma)$, valid for small distortions and correct to second order in y_γ ,

$$n(x, y_\gamma) = n_{\text{pl}} + y_\gamma \Delta T_e n_y + \frac{y_\gamma^2}{2} \left[\Delta T_e f_y(x) + \Delta T_e^2 f_2(x) + \frac{\partial \Delta T_e}{\partial y_\gamma} n_y(x) \right] + \mathcal{O}(y_\gamma^3), \quad (\text{B.4})$$

where ΔT_e and its derivative are evaluated at $y_\gamma = 0$.

The last term, $\frac{\partial \Delta T_e}{\partial y_\gamma}$, depends on the physics responsible for the electron temperature T_e . It is also clear that higher order terms will have higher order derivatives of ΔT_e and the above solution is only valid when these higher order derivatives are negligible compared to the first derivative. We will ignore this term in the rest of this section, as it is not relevant to the present discussion. In the early Universe, however, electron temperature is not constant and changes as comptonization progresses and we will discuss the evolution of the electron temperature in detail in the next sections. If the electrons are in equilibrium with radiation, $\frac{\partial \Delta T_e}{\partial y_\gamma}$ is easily calculated by taking derivative of Eq. (5.1).

We can now use the fact that the blackbody spectrum is a steady state solution of the Kompaneets equation.

$$\begin{aligned} n(x, 0) + n(x, 0)^2 &= -\frac{\partial n(x, 0)}{\partial x} \\ &= -\frac{\partial n(x, y_\gamma)}{\partial x} + y_\gamma \frac{\partial^2 n}{\partial y_\gamma \partial x}(x, 0) + \frac{y_\gamma^2}{2} \frac{\partial^3 n}{\partial y_\gamma^2 \partial x}(x, 0) \\ &\quad + \mathcal{O}(y_\gamma^3) \end{aligned} \quad (\text{B.5})$$

We have used Eq. B.1 in the last step. Using again the expansion Eq. B.1 and Eq. B.5 in the Kompaneets equation to replace $n + n^2$ term and , we get, on ignoring terms of order y_γ^3 and higher,

$$\begin{aligned} \frac{\partial n(x, y_\gamma)}{\partial y_\gamma} &= \frac{1}{x^2} \frac{\partial}{\partial x} \left[x^4 \left(\frac{\partial n(x, y_\gamma)}{\partial x} \left(\frac{T_e}{T} - 1 \right) \right. \right. \\ &\quad \left. \left. + y_\gamma \left(\frac{\partial^2 n}{\partial y_\gamma \partial x}(x, 0) + \frac{\partial n}{\partial y_\gamma}(x, 0) + 2n(x, 0) \frac{\partial n}{\partial y_\gamma}(x, 0) \right) \right. \right. \\ &\quad \left. \left. + \frac{y_\gamma^2}{2} \left(\frac{\partial^3 n}{\partial y_\gamma^2 \partial x}(x, 0) + \frac{\partial^2 n}{\partial y_\gamma^2}(x, 0) + 2n(x, 0) \frac{\partial^2 n}{\partial y_\gamma^2}(x, 0) \right. \right. \right. \\ &\quad \left. \left. \left. + 2 \left(\frac{\partial n}{\partial y_\gamma}(x, 0) \right)^2 \right) \right] \right] + \mathcal{O}(y_\gamma^3) \end{aligned} \quad (\text{B.6})$$

We are interested in the behavior of corrections as y_γ and ΔT_e increase. Thus collecting all terms of same order in y_γ and ΔT_e (and defining representing x -dependence with functions $F_n(x)$ for brevity)⁶, we have

$$\begin{aligned} \frac{\partial n(x, y_\gamma)}{\Delta T_e \partial y_\gamma} &\equiv \frac{1}{x^2} \frac{\partial}{\partial x} \left[x^4 \frac{\partial n(x, y_\gamma)}{\partial x} \right] + y_\gamma F_1(x) + y_\gamma^2 F_2(x) + y_\gamma^2 \Delta T_e F_3(x) \\ &\quad + \mathcal{O}(y_\gamma^3) \end{aligned} \quad (\text{B.7})$$

$$\begin{aligned} \stackrel{x \gg 1}{\approx} &\frac{1}{x^2} \frac{\partial}{\partial x} \left[x^4 \frac{\partial n(x, y_\gamma)}{\partial x} \right] - (2y_\gamma x^3 - 3y_\gamma^2 x^4 + 2y_\gamma^2 \Delta T_e x^5) n_{\text{pl}}(x) \\ &\quad + \mathcal{O}(y_\gamma^3) \end{aligned} \quad (\text{B.8})$$

⁶We only give the $x \gg \text{limit}$ below but the functions $F_n(x)$ just involve the Planck function n_{pl} and its derivatives are easily calculated explicitly if desired.

The last expression illustrates clearly the regime of validity of the y -type solution. The y -type solution is valid in the limit $y_\gamma \ll 1$ and $y_\gamma^2 \Delta T_e \ll 1$. Also the solution fails at $x \gg 1$, when the recoil effect gives deviations of order unity with respect to the blackbody. The recoil effect would lead to a downward shift in the frequency of high energy photons given by $1/x' - 1/x = y_\gamma$ [80, 81]. Thus the y -type solution is only valid for $x \ll 1/y_\gamma$. This is also easily seen by comparing the first term on the right hand side ($\sim x^2 n_{\text{pl}}$) with the first two terms in round brackets, $(2y_\gamma x - 3y_\gamma^2 x^2)x^2 n_{\text{pl}}$ in the limit $x \gg 1$.

In particular for $\Delta T_e \ll 1$, as is the case in the early Universe before recombination, the $y_\gamma \ll 1$ is the stronger condition. Thus the y -type solution is the correct solution for energy injection at $z \lesssim 20000$ with the corrections due to higher order terms of the order $\sim y_\gamma \sim 10^{-2}$ (Fig. 4).

With $y = \int_0^{y_\gamma} \Delta T_e dy_\gamma$ and $y \ll 1$, an approximate linear solution of Eq. (B.7) follows by evaluating the right hand side of Eq. (B.7) at $y_\gamma = 0$, with $y = 1/4(\Delta E/E_r)$, ΔE is the energy injected into the plasma and E_r is the initial radiation density.

$$\begin{aligned} n(x, y) - n_{\text{pl}}(x) &= y n_y(x) \\ &= y \frac{x e^x}{(e^x - 1)^2} \left[x \frac{e^x + 1}{e^x - 1} - 4 \right] \end{aligned} \quad (\text{B.9})$$

An important difference between Eq. (B.9) and linear + second order $d\Delta T_e/dy_\gamma$ term in Eq. (B.4), although they look identical, is that in Eq. (B.9) we have defined y as an integral over ΔT_e and there is no restriction on the higher order derivatives of ΔT_e , except that the integral $y \ll 1$ and the assumptions under which Kompaneets equation is derived are valid. We have in effect summed over all the terms coming from the Taylor series expansion of ΔT_e in Eq. (B.4). The solution in Eq. (B.9), written in terms of y , is thus, more generally applicable. This solution is valid for $\Delta n/n_{\text{pl}} \ll 1$, which implies that for large x we have the condition $x^2 y \ll 1$. This condition is clearly satisfied for the CMB, with the current limit of $y < 10^{-5}$, in the Wien tail for $x < 100$. The well known solution Eq. (B.9) [3] depends only on y and not on y_γ . The next correction depends also on y_γ . This demonstrates that the broadening of the spectrum and redistribution of photons over the frequency is defined by T_e but the energy exchange between the plasma and the radiation is defined by $T_e - T$.

C Corrections to y -type distortion from weak comptonization and recursion relations for calculating the higher order terms

The solution to the Kompaneets equation for small distortions, with the initial spectrum being a blackbody spectrum, for small values of y_γ parameter, $y_\gamma \ll 1$, is given by the Taylor series Eq. (B.1), with the first two coefficients/derivatives given by Eqs. (3.4) and (B.3). The functions $f_y(x)$ and $f_2(x)$ just involve derivatives of the Planck spectrum and are easily calculated.

$$\begin{aligned} f_y(x) &= \frac{-2e^x x}{(e^x - 1)^5} \left[-x^2 - 7x - 8 + e^{3x} (x^2 - 7x + 8) \right. \\ &\quad \left. + e^x (-2x^3 - 9x^2 + 7x + 24) + e^{2x} (-2x^3 + 9x^2 + 7x - 24) \right] \end{aligned} \quad (\text{C.1})$$

$$\begin{aligned} f_2(x) &= \frac{e^x x}{(e^x - 1)^5} \left[x^3 + 12x^2 + 34x + 16 + e^{3x} (x^3 - 12x^2 + 34x - 16) \right. \\ &\quad \left. + e^{2x} (11x^3 - 36x^2 - 34x + 48) + e^x (11x^3 + 36x^2 - 34x - 48) \right] \end{aligned} \quad (\text{C.2})$$

For an initial y -type spectrum, $n(x, 0) = n_{\text{pl}}(x) + y n_y(x)$, $\Delta T_e(y_\gamma = 0) = 5.4y$, we can similarly expand the solution $n(x, y_\gamma)$ in Taylor series, keeping only terms linear in y since COBE/FIRAS [1]

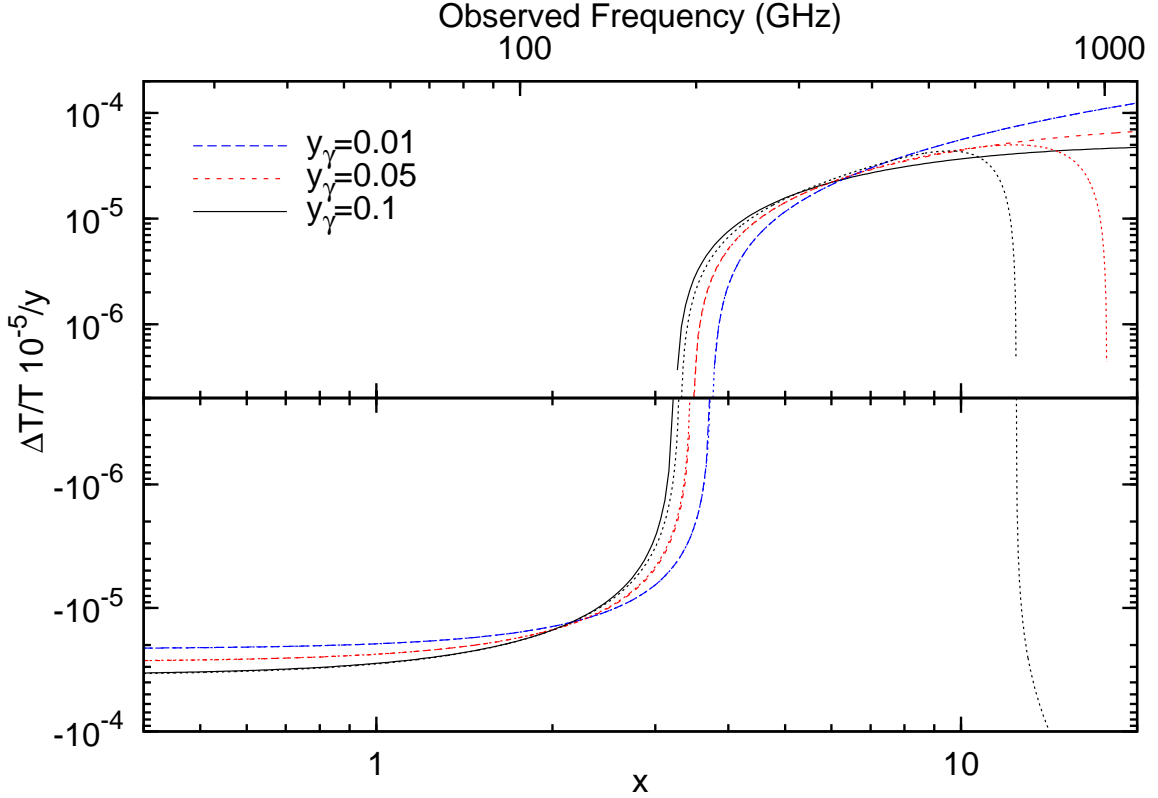


Figure 16. Analytic solution given by Eq. (C.4) including terms up to y_γ^3 is shown by dotted lines for $y_\gamma = 0.01, 0.05, 0.1$ from top to bottom (in the Rayleigh-Jeans and Wien tails) respectively. Numerical solutions are as marked. Fractional difference in the effective temperature, Eq. (3.5), is plotted. The two solutions match well for $y_\gamma \ll 1$ and $x \ll 1/y_\gamma$. At $y_\gamma = 0.1$ the analytic solutions has the correct approximate shape. Errors are plotted in Fig. 17

already constrains the average cosmological distortion. $y \lesssim 10^{-5}$, y_γ on the other hand covers a wide range and is > 1 at $z > 1.45 \times 10^5$. y_γ in the solutions refers to the total y_γ integrated from the time of energy injection to the time where we want to calculate the final distortion.

$$n(x, y_\gamma) = n_{\text{pl}}(x) + y n_y(x) + y_\gamma \frac{\partial n}{\partial y_\gamma}(x, 0) + \frac{y_\gamma^2}{2} \frac{\partial^2 n}{\partial y_\gamma^2}(x, 0) + \frac{y_\gamma^3}{6} \frac{\partial^3 n}{\partial y_\gamma^3}(x, 0) + \mathcal{O}(y_\gamma^4) \quad (\text{C.3})$$

We can calculate the coefficients in Taylor series iteratively by using Kompaneets equation. The first derivative is thus given by the Kompaneets equation. Second derivative is obtained by differentiating Kompaneets equation with respect to y_γ and using the solution of first derivative and so on. Derivatives of $\Delta T_e(y_\gamma)$ are also easily obtained using Eq. (5.1). First two derivatives are $d\Delta T_e/dy_\gamma|_{y_\gamma=0} \approx -21.45y$, and $d^2\Delta T_e/dy_\gamma^2|_{y_\gamma=0} \approx 323.6y$. Thus,

$$n(x, y_\gamma) = n_{\text{pl}} + y \left[n_y + y_\gamma (5.4n_y + f_y) + \frac{y_\gamma^2}{2} (-21.45n_y + 5.4f_y + g_y^{(2)}) + \frac{y_\gamma^3}{6} (323.6n_y - 21.45f_y + 5.4g_y^{(2)} + g_y^{(3)}) \right] + \mathcal{O}(y_\gamma^4). \quad (\text{C.4})$$

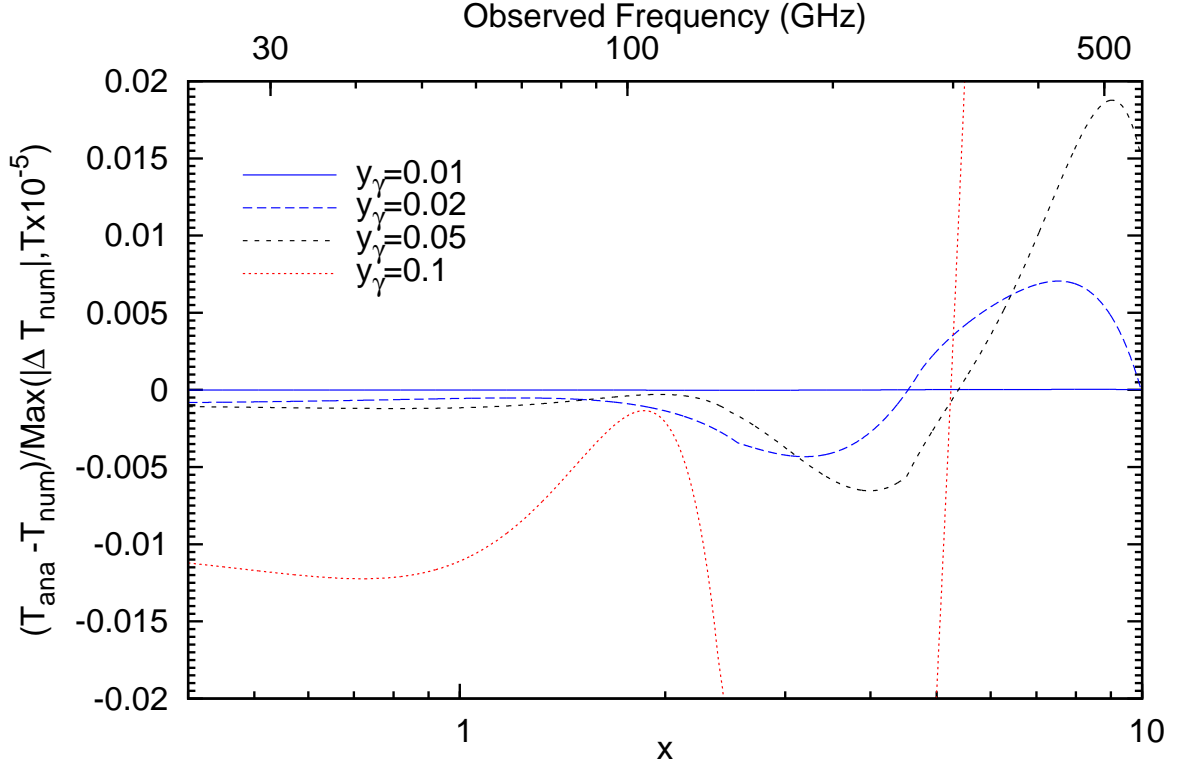


Figure 17. Error in analytic solution defined by $\frac{(\Delta T/T)_{\text{analytic}} - \Delta T/T_{\text{numerical}}}{\max(|\Delta T/T|_{\text{numerical}}, 10^{-3})}$. The analytic solution has better than 1% accuracy over most of the frequency range of interest at $\gamma_y \lesssim 0.05$. Accuracy deteriorates quickly at larger values of γ_y .

In general m^{th} derivative is given by (for $m > 1$),

$$\frac{\partial^m n}{\partial y_\gamma^m}(x, 0) = \sum_{i=0}^{m-1} \frac{1}{y} \frac{d^i \Delta T_e}{dy_\gamma^i} g_y^{(m-i-1)} + g_y^{(m)}, \quad (\text{C.5})$$

where $g_y^{(0)} = n_y$, $g_y^{(1)} = f_y$ and for $m > 0$ the $g_y^{(m)}$ functions are given recursively by

$$g_y^{(m+1)} = \frac{1}{x^2} \frac{\partial}{\partial x} x^4 \left(\frac{\partial g_y^{(m)}}{\partial x} + g_y^{(m)} (1 + 2n_{\text{pl}}) \right). \quad (\text{C.6})$$

We compare the the analytic solution including first three terms (up to order y_γ^3) and the numerical solution in Fig. 16. The two solutions match very well for $y_\gamma \ll 1$, $x \ll 1/y_\gamma$ and the error at $y_\gamma = 0.05$ is $\lesssim 1\%$ for $x \lesssim 7$. However, for larger values of y_γ , the solution quickly deteriorates, and at $y_\gamma = 0.1$ the error is of order 10% at $x \lesssim 6$. For $y_\gamma \lesssim 0.01$, the linear order term is enough to give $\sim 1\%$ accuracy. Fig. 18 compares the analytic solution including up to linear, quadratic and cubic terms with numerical solution for $y_\gamma = 0.1$. It can be seen that with the inclusion of successive terms, the analytic solution oscillates around the true solution and convergence is quite slow. Table 1 gives the approximate maximum values of y_γ where the error at $x \lesssim 6$ is below 1%, 5%, 10% at linear, quadratic and cubic orders in y_γ .

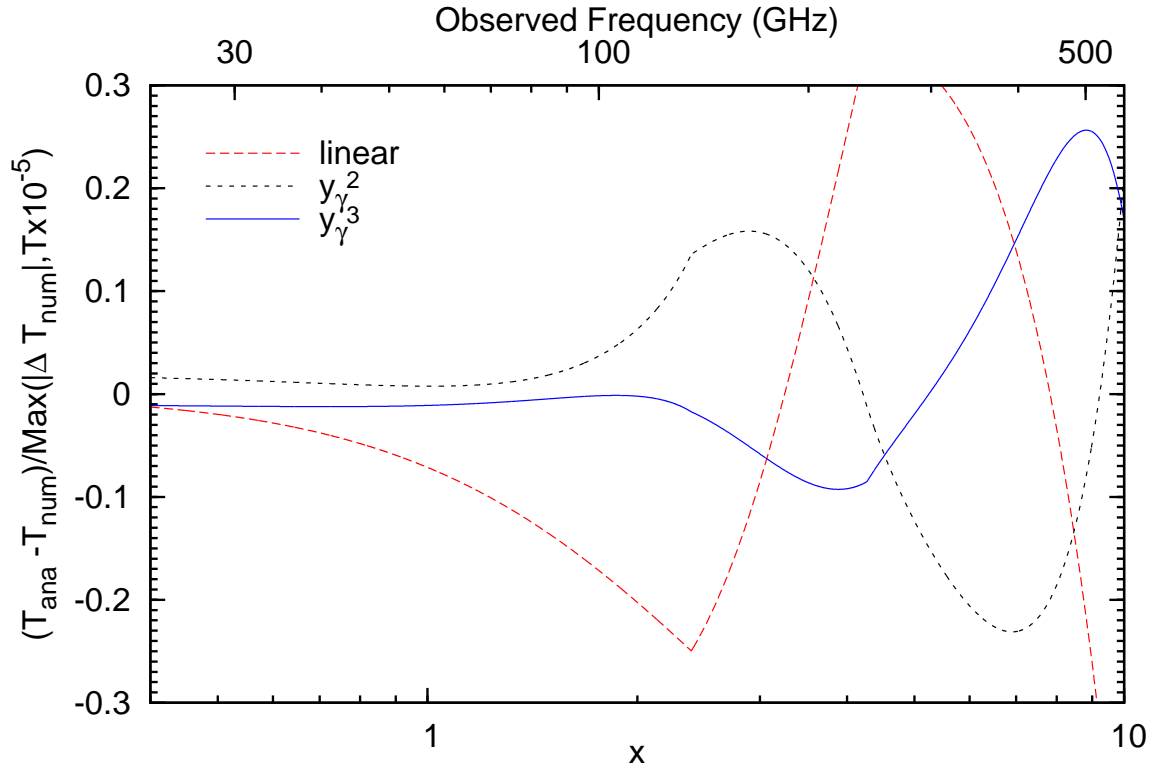


Figure 18. Error in analytic solution defined by $\frac{(\Delta T/T_{\text{analytic}} - \Delta T/T_{\text{numerical}})}{\max(|\Delta T/T_{\text{numerical}}|, 10^{-5})}$ for $y_\gamma = 0.1$ for analytic solutions at different orders. The analytic solution has better than 10% at $x \lesssim 6$. It can be seen that the convergence of the Taylor series is very slow at $y_\gamma = 0.1$ with the analytic solution oscillating around the true solution with inclusion of successive terms.

Error	1%	5%	10%
linear	0.01	0.03	0.04
quadratic	0.03	0.06	0.08
cubic	0.05	0.08	0.1

Table 1. Upper bound on errors in the analytic solutions at different orders in y_γ . The upper bounds in different columns are reached at the values of y_γ shown. This table can be used as a rough guide when using analytic solutions.